TIROS III METEOROLOGICAL SATELLITE RADIATION OBSERVATIONS OF A TROPICAL HURRICANE

(NASA TM X-50668)

by

W. R. Bandeen, V. Kunde,
W. Nordberg and H. P. Thompson

Goddard Space Flight Center

22 refs (Submitted for Publication)

1. Introduction

The first of the TIROS series of meteorological satellites whose active lifetime extended over the peak of the Atlantic hurricane season was TIROS III. Launched on 12 July 1961, TIROS III carried a two-camera, quasi-operational television system which observed every hurricane of the 1961 season. TIROS III also carried an experimental medium-resolution radiometer, scanning the earth and its atmosphere in five regions of the electromagnetic spectrum which gathered data from the same storms from an orbital height of about 780 km.

The design of the radiometers, their calibration, the information flow, and the data reduction techniques have been described previously[2,17,7]. The physical significance of the experiment and its synoptic use potential have also been discussed earlier[8,6].

In this paper, we shall describe the radiation patterns observed in five intervals of the solar and terrestrial spectrum over "Anna", the first Atlantic hurricane of 1961. This description presented in the color maps, Figures 1 to 13, is based on automatically processed data telemetered from the TIROS III

Available to NASA Offices and

X63 15689
N65-88838
Code 2A

56p

15689

ABSTRACT

(NASA TMX 50668)

On July 12, 1961, the TIROS III meteorological satellite (1961 rho 1) was launched carrying two television cameras and a family of radiation sensors in the visible and infrared portions of the spectrum. During the period July 18-24, the first hurricane of the 1961 Atlantic season, Hurricane Anna, was observed clearly by a five-channel medium resolution radiometer on the satellite as well as by the television cameras. Data gathered by the radiometer during this period are presented in the form of maps, together with supporting television pictures. The possibility of infer stratospheric water vapor content above the hurricane by comparing measurements from the 5.9-6.7 micron water vapor and the 7.5-13.5 micron window channels is investigated. We have concluded that only very limited inferences can be made because of our insufficient knowledge of the transfer of radiation at low pressures and in the cloud-atmosphere interface and because of insufficient accuracy of the sensors flown in TIROS III.

NASA Centers Only

satellite. We shall also discuss the possibility of inferring the stratospheric water vapor content over the hurricane by comparing measurements from two different channels.

2. Design of the Experiment

To aid in understanding the radiation maps shown, the basic characteristics of the radiation sensors will be reviewed. The medium-resolution radiometer flown in TIROS III is practically identical to the first of its kind flown in TIROS II. There are five channels in the radiometer, each sensitive to a different part of the electromagnetic spectrum by the use of filters and other optical elements. The nominal bandwidths of the five channels are:

Channel 1	5.9-6.7 microns, water vapor absorption
Channel 2	7.5-13.5 microns, atmospheric window
Channel 3	0.2-7.0 microns, reflected solar radiation
Channel 4	7.0-32.0 microns, terrestrial radiation
Channel 5	0.5-0.75 microns, response of TV system

The radiometer employs a chopper which causes each sensor, consisting of a thermistor bolometer and associated optics, to view alternately, and at a rapid rate, in two directions 180 degrees apart. The response of each sensor is proportional to the difference in the irradiation of the sensor from the two directions. The optical axes of the sensors are nearly parallel to one another and inclined to the spin (TV camera) axis by 45 degrees. The satellite spins at about 9.3 rpm, causing the field of view to scan over the earth and space.

When viewing directly downward from a height of 780 km, the "spot" on earth viewed by the radiometer has a diameter of about 68 km. As the nadir angle increases, the scan spot becomes increasingly elongated in the direction viewed. TIROS is spin

stabilized, and as it revolves in orbit, the radiometer scan geometry over the earth passes through a sequence of rather complicated patterns. However, in any configuration, at least one direction of the sensors must always view outer space, which establishes the necessary reference level for each of the five spectral regions.

3. Calibration

The calibration of the three infrared sensors [18] is carried out by simulating the outer space reference and the earth signal for each viewing direction respectively in the laboratory. The field of view of the radiometer in one direction is filled by a blackbody target at liquid nitrogen temperature (80°K), which is essentially equivalent to the space reference, while the field of view in the other direction is filled with a blackbody target whose temperature is varied over the range expected when viewing the earth and its atmosphere. Thus, the radiant emittances measured by the satellite and shown on the maps for these three channels are expressed in terms of an "equivalent temperature", T_{BB}, in degrees K of a blackbody filling the field of view which would cause the same response from the radiometer.

In the calibration for solar radiation [18], one direction of each sensor is merely masked with black tape to simulate space. To simulate reflected solar radiation from the earth and its atmosphere, a white diffuse reflector of known spectral reflectivity is illuminated at normal incidence by a standard lamp of known spectral intensity at a measured distance away, thus determining the spectral radiant emittance from the reflector. With the illuminated reflector filling the field of view, the output signal from each sensor is measured. The

spectral radiant emittance from the reflector is integrated over the spectral response curves of each sensor to yield that portion of the radiation viewed to which each sensor responds. The result of such integration is the "effective radiant emittance", $\overline{W}$. Thus the measurements of reflected solar radiation are expressed in terms of that portion of the radiant emittance, in watts per square meter, to which each sensor responds. It is stipulated that the radiation originates from a diffuse target completely filling the field of view of the sensor. In order to interpret these measurements in terms of reflectance of insolation (or loosely "albedo"), one must know the effective radiant emittance, $\overline{W}^*$, which would be measured by each sensor if the field of view were filled by a diffuse reflector of unit reflectivity when illuminated by one solar constant at normal incidence. The values of $\overline{W}^*$ for channels 3 and 5 have been calculated to be, respectively, 763.8 watts m^{-2} and 108.6 m^{-2} watts.

4. Construction of the Maps

The maps shown in Figures 1-13 were produced by automatic data processing techniques, with the exception of the shading between contours which was done manually to enhance the display. Figure 2b was specially produced at a scale twice as large as in the other maps, and the isotherms were hand-traced and labeled to increase resolution in displaying the data.

In producing the maps in Figures 1-5 (except 2b), a computer program selected all data having a sensor nadir angle of 58 degrees or less during the time period 1545 GMT to 1602 GMT, 21 July 1961, averaged all data points falling within a Mercator Projection grid element with a mesh interval of 2.5 degrees of longitude (about 278 km square at the equator), and

printed the average value for each grid element at the appropriate location on the map. Figure 2b was produced in the same way, except that data from 1545 GMT to 1557 GMT were used and the mesh interval was 1.25 degrees of longitude, thus increasing the area resolution by a factor of four. In Figures 1-13, the computer produced contours were shaded manually to enhance the contrast in the presentation. The sub-satellite track is shown with sub-satellite points indicated for each minute of time. That the camera principal pointtrack lay southwest of the sub-satellite track is evidenced by the displacement of the data center of mass with respect to the sub-satellite track. The minimum spin (television camera) axis nadir angle was 16.0 degrees and occurred at 1558:30 GMT.

The "composite" maps in Figures 6-13 were produced for the indicated time periods from two or three consecutive orbits in the same fashion as the maps in Figures 1-5 described above, but with a limiting nadir angle of 56°. The 56 degree nadir angle threshold was chosen after some experimentation to provide perfect contiguity between adjacent orbits. Only data from the atmospheric window and the narrow band solar channel are shown in the composite maps. The data from each orbital pass run from the northwest to the southeast (cf. Figures 1-5) with the higher numbered orbits positioned increasingly westward due to the earth's rotation. The latitudinal gaps near 10°S in the data of Figures 6-11 result from the inability of the automatic data processing system to cope in this case with a particular scanning mode called the "closed mode". The "closed mode" occurs whenever the spin axis nadir angle is less than about 17.0 degrees (or greater than its antipodal value, 163.0 degrees), under which conditions the radiometer sensors never scan across the horizon

but scan continuously the earth throughout a complete rotation of the satellite. In contrast to the "open mode" where the radiometer sensors scan the earth from horizon to horizon for a portion of each rotation of the satellite such that there are two horizon pulses available for spin synchronization in every scan, in the "closed mode" the spin coordinate must be extrapolated by the computer for a period of about ten minutes. This extrapolation is extremely sensitive to error propagation, and, consequently, in many orbits it is observed that closed mode data spots are mislocated on earth due to accrued spin coordinate errors. While these mislocation errors of the order of several hundred miles would generally be negligible in large scale analyses (e.g. the planetary heat balance), they cause "smearing" of the images of such observed features as the cloud systems associated with individual storms. For this reason, the closed mode data were eliminated in Figures 6-11. In Figures 12 and 13 there are no latitudinal gaps because by 24 July 1961 the satellite spin vector had turned out of the orbital plane by 21.5 degrees and, hence, there were no closed mode data. In Figures 1-5, a small amount of closed mode data is included south of the equator. However, it was determined by a separate manual analysis that the closed mode data in this case did not appreciably affect any of the pattern images and hence the data were left intact.

Figures 1-13 include examples of all orbits where cloud systems associated with Hurricane Anna can be clearly identified. Unfortunately, some data of interest were either not available e.g., orbit 88 on 18 July (cf. Figures 6 and 7) and all orbits on 22 and 23 July. The population of measurements within a grid element varies from 1 along the southwestern edge to more than

60 (or about one-fourth of this number for Figure 2b) along the northeastern edge of an orbital area. This large variance results from the complicated geometry of the scan.

After the computer averages the individual measurements within each grid element, it contours the grid point averages with filler numbers, and prints the maps on a high speed printer. Replacing the filler numbers by manually shading between contour intervals (or tracing the isotherms in Figure 2b) produced the maps shown in Figures 1-13. The data in these figures are also available in unanalyzed grid print form at a higher resolution [19]. Two limitations of the map form of data display are re-emphasized, viz., (1) the direction from which a measurement is made (i.e., nadir or zenith and azimuth angles), and (2) the number of individual measurements making up each grid point average (or the amount of data smoothing) are not readily apparent. These limitations must be kept in mind when attempting to interpret such maps.

5. Discussion of the Maps

Hurricane Anna moved from a point just north of Venezuela to the coast of British Honduras during the period 20-24 July 1961. At 1550 GMT on July 21, Anna was centered at latitude 13.8°N, longitude 72.3°W, and was still growing in intensity. Orbit 132 of TIROS III passed almost directly over the hurricane at that time, and the attitude of the satellite was such that all radiometer measurements over Anna were made under sensor nadir angles of less than 15 degrees. Figures 1-5 show the stark relief in which the hurricane stands out from its surroundings in all five spectral regions. For comparison, in Figures 14-15 two television pictures taken by TIROS III at about the same time the radiation data were acquired show Anna, the extensive

cloudiness just to the south of it, and the scattered-to-clear regions over equatorial South America.

Figure 14 shows Anna centered about 70 miles north of the Guajira Peninsula, with the Colombian coastline running laterally to the west and joining Panama. Lake Maracaibo is cradled in the upper right-hand quadrant of the central fiducial cross. A second extensive cloud system is seen south of Anna over Venezuela. The temperatures shown in Figures 2 and 4 clearly outline this second system and indicate that its mean top is at a lesser height than the hurricane. Also, the increased temperatures on these maps over the region stretching from Venezuela to Peru indicate that the band of clouds shown for this region on the reflected solar radiation maps (Figures 3 and 5) is at a still lower height, or is thinner, or both.

The hurricane stands out clearly in both solar radiation channels. The observed upper limits for grid element averages for $\bar{W}$ over the hurricane are 240 watts/meter^2 and 40 watts/meter^2, respectively, for channels 3 and 5. The subsolar point at 1550 GMT was latitude 20.4^{o}N, longitude 55.9^{o}W, some 18 degrees from the storm center. Taking the solar radiation incident upon the hurricane as $\bar{W}^*$ cos 18^o, the reflectance of sunlight in the direction of the satellite may be determined by a simple ratio. However, there is evidence that between the time of the original calibration and launch day, the response of channel 3 degraded to about 0.75 of its calibrated level and that between launch day and orbit 132 it degraded still further to about 0.69 of its calibrated level. On the other hand, although no pre-launch degradation was observed in channel 5, an appreciable post-launch degradation was observed amounting to about 0.85 of its calibrated level by orbit 132. The reasons for these degradations

are not yet fully understood. Since there is no satisfactory on-board calibration of the TIROS radiometer, the post-launch degradation estimates have been based upon a statistical treatment of large quantities of data using the earth itself as a calibration target. Therefore, incorporating the above correction factors, the upper limits of the reflectance, r, over the hurricane shown on the maps become

$$\text{Channel 3:} \quad r = \frac{240}{763.8(\cos 18^{o})} \cdot \frac{1}{0.69} = 47.9\% \qquad (1)$$

$$\text{Channel 5:} \quad r = \frac{40}{108.6(\cos 18^{o})} \cdot \frac{1}{0.85} = 45.7\% \qquad (2)$$

In interpreting these values, one should remember that they are averages of a large number of "spots", smoothed over thousands of square kilometers, and that the reflectances of the individual spots are both higher and lower than the grid point averages. For example, the maximum reflectances calculated from individual spots over the hurricane (including the degradation corrections) were 73% and 69%, respectively, for channels three and five.

The patterns in the maps for both solar radiation channels are very similar. The large cloud system south of the hurricane over Venezuela and the band of cloudiness stretching from it southwest across Colombia into Northern Peru stand out clearly in Figures 3 and 5, and can be identified in the television pictures in Figures 14 and 15. The high reflectance region around 22°S and 63°W infer the presence of clouds, but the

relatively high temperatures measured by channel 2 indicate that the cloud tops were not very high. The broad band of high channel 2 temperatures running from the Amazon basin across Brazil to the Atlantic Ocean compares well with the low value measured for reflected solar radiation, inferring the absence of cloudiness and indicating that the radiation sensed in the window channel emanated near the surface. The channel 4 and channel 1 maps also show a similar pattern, and the photograph in Figure 15 confirms the scattered-to-clear condition over the Amazon region of Brazil.

In Figure 2a/ values of T_{BB} below 240°K are shown for the region north of latitude 30°N off Florida for channel 2. Widespread cumulonimbus clouds with anvil tops were reported in this region at the time, and undoubtedly contributed to the low temperatures observed. However, a complication in interpreting measurements in this region is that they were all made under nadir angles of nearly 58°. The comparable zenith angles at the top of the atmosphere were about 72°, meaning that the radiometer was viewing along a path of more than three atmospheres. Under these conditions, appreciable limb darkening plus the possibility of space beyond the horizon being contained in the field of view might contribute to the observed low temperatures in addition to high cloudiness.

On 17 July 1961, TIROS III photographs indicated a concentration of cloudiness near 12°N, 43°W, and Navy reconnaissance noted an extensive area of strong radar echoes well to the east of the Windward Islands. Figures 6-13 in conjunction with Figures 1-5 illustrate the ability of both infrared and reflected solar radiation measurements to locate and track storm systems. For comparison, Table I lists approximate locations

of the storm as derived from conventional data [1] and from Figures 1-13. It can be seen that the locations derived from the satellite radiation data complement well the conventionally determined storm positions. Figures 6 and 7 locate the incipient storm at about 12.0°N, 49.0°W at 1600 GMT on 18 July.

TABLE 1

Locations of Hurricane Anna Derived from Conventional Data Compared with Locations Derived from Radiation Data

Date (1961)	Time (GMT)	Lat (°N)	Long (°W)
18 July	1600 (Fig. 6, 7)	12.0	49.0
19 July	1520 (Fig. 8, 9)	11.0	58.0
20 July	0000	11.5	60.2
20 July	1200	11.9	63.8
20 July	1440-1645 (Fig. 10, 11)	11.5	65.5
21 July	0000	13.0	67.6
21 July	1200	13.4	71.5
21 July	1550 (Figs 1-5)	13.8	72.3
22 July	0000	13.7	74.8
22 July	1200	14.5	78.2
23 July	0000	15.2	81.4
23 July	1200	15.8	84.3
24 July	0000	16.1	86.7
24 July	1200	16.6	88.3
24 July	1541 (Fig. 12, 13)	17.5	89.0

Figures 8 and 9 locate the storm at about 11.0°N, 58.0°W at 1520 GMT on 19 July. In Figures 10 and 11, the storm was observed by both orbits 117 and 118 near the southwestern and northeastern edges respectively of their data areas. The image of the storm

resulting from a composite of data in the overlap region of the two orbits is apparently distorted near 11.5°N, 65.5°W, due to the storm's motion between about 1440 GMT and 1625 GMT on 20 July. The winds in the storm reached hurricane velocities about this time. Figures 1-5 locate the hurricane at 13.8°N, 72.3°W at 1550 on 21 July. There were no reducible data on 22 or 23 July, but Figures 12 and 13 locate the dissipating storm at about 17.5°N, 89.0°W over British Honduras at 1541 GMT on 24 July.

The composite maps of both channels outline the July Intertropical Convergence Zone near 10°N and give evidence of a clear winter subtropical zone in the southern hemisphere, although from this aspect, it is especially unfortunate that the closed mode data are missing.

All of the reflected solar radiation maps exhibit a rather remarkable characteristic. There are vast regions where the reflectances measured by the radiometer are uniformly low, yielding values of less than 10% calculated as in equations (1) and (2). In fact, the average reflectance values of all maps, even after applying our estimated corrections for instrumental degradation, falls in the region 15% to 20%, or about half of the generally accepted albedo of the earth. Of course, such a small sample over a limited region of the globe does not permit the drawing of general conclusions regarding the planetary albedo, but the inferences set forth a clear challenge for concerted work in this area, utilizing present and future satellite radiation data.

6. Discussion of Possible Inferences from Coordinated Measurements from Channels 1 and 2

It is to be expected that an analysis of coordinated measurements by two (or more) channels should yield information not

obtainable from any single channel. One application of this type arises from coordinated observations in the water vapor absorption channel 1 and the window channel 2. Möller has proposed a method for estimating the relative humidity of the upper troposphere and the temperature of the ground or of the clouds from comparisons of measurements made by these two channels [15]. In a previous paper [3], three of us suggested that the water vapor content of the stratosphere over a large storm whose cloud tops extend to the vicinity of the tropopause could be inferred from coordinated channel 1 and channel 2 measurements. The attempted application of this hypothesis to Hurricane Anna has pointed up several factors which seem to preclude a successful test of the method at this time. We shall discuss these factors together with a brief review of the original concept below.

Each infrared channel "sees" many different layers in the atmosphere. The contribution of each atmospheric layer to the integrated response of a particular channel depends upon the vertical distributions of temperature, pressure, and the various infrared absorbers (primarily H_2O, CO_2, and O_3), and upon the positions and strengths of the various absorption bands with respect to the spectral response curve of the particular channel. Because of strong absorption of water vapor in the 6.3 micron band, generally (in the absence of clouds) a broad region throughout the middle and upper troposphere predominates in contributing to the response of channel 1, with little or no contribution from the surface of the earth.

Because of only weak absorption by ozone and water vapor in the atmospheric window. radiation from the surface of the earth or from clouds predominates in the response of channel 2,

with small contributions from the atmosphere. Because channel 4 includes the window as well as strong water vapor and carbon dioxide absorption bands, it receives important contributions from both earth and atmosphere. The air temperature generally decreases with height in the troposphere where a preponderance of the important absorbers is found; hence, it follows that usually the equivalent blackbody temperatures, T_{BB}, measured by channel 1 should be lowest, those measured by channel 2 highest, and those measured by channel 4 somewhere between the first two. This pattern generally prevails throughout Figures 1, 2, and 4 with channel 1 temperatures 20^{o} to 40^{o}K lower and channel 4 temperatures 10^{o} to 20^{o}K lower than the channel 2 values of T_{BB}. The one exception to this pattern is over the hurricane, where the T_{BB} values for all channels are indicated as 220^{o}-230^{o}K.

If we define a fictitious level, called the "effective height of radiation", as the height at which the T_{BB} measured by the satellite corresponds to the real atmospheric temperature, it follows from the previous paragraph that the effective height of radiation from channel 1 should be highest and that for channel 2 lowest, with the channel 4 height falling in between. Fritz and Winston [6] have shown that the effective height of radiation for the window channel of TIROS II affords a good estimate of the heights of the tops of large-scale overcast clouds, although cirrus are not clearly defined because they are partially transparent.

From radiosonde data taken near the hurricane, the ambient air temperature ranged from 230^{o} to 220^{o}K in the height interval from about 11,000 to 12,100 meters, inferring that the smoothed mean height of the hurricane clouds as mapped in Figure 2 lay within this layer. However, the smoothing contained in the

grid point averages and the 10°K contour intervals used in the maps obscure much of the fine structure which is possible within the 5 degree instantaneous field of view of the instrument.

For example, a computer listing of the individual data points making up the maps revealed several individual spots (remembering that a spot diameter on earth is about 68 km) over the hurricane, where there was a dramatic reversal of the usual order of T_{BB} measurements from the infrared channels coincident with the minimum observed channel 2 temperatures. Three of these spots, each from a different swath, yielded the following values of T_{BB} (cf. Reference 7, pp. 291-292):

TABLE 1

Reversal of the Usual Order of Infrared Channel Equivalent Blackbody Temperatures in Three Spots Over Hurricane Anna

	T_{BB} (Uncorrected)		
	Spot 1 (°K)	Spot 2 (°K)	Spot 3 (°K)
Channel 1 (5.9-6.7 microns)	229.6	232.0	231.5
Channel 4 (7.0-32.0 microns)	223.9	217.0	217.0
Channel 2 (7.5-13.5 microns)	208.4	213.3	211.9
ΔT_{BB} = (Chan.1 T_{BB}-Chan.2 T_{BB}) =	+21.2°K	+18.7°K	+19.6°K

Even more dramatic are the analog traces of the raw data as they were telemetered to the ground from the satellite. In Figure 16 the analog traces from channel 1 and channel 2 during one swath over the hurricane are superimposed. The minimum

channel 2 T_{BB} = 197°K (uncorrected) is the lowest measurement recorded over the hurricane, resulting in a difference, ΔT_{BB}, between the equivalent blackbody temperatures of channel 1 and channel 2 of 223.5-197.0 = 26.5°K (uncorrected). Normally, in processing the data by a computer, a sample is taken every 0.1309 seconds. Figure 16 illustrates how the sharp dips and peaks can be missed in the normal computer processing if they fall between samples, e.g., the lowest channel 2 T_{BB} appearing in the computer listing is 208.4°K (cf. Table 1 and Figure 17). (Actually the channel 2 signal in Figure 16 dropped so low that the logic of the computer program failed, and, in this swath only, the data over the hurricane were rejected in the automatic processing.)

The temperature and height of the tropopause averaged from 1200Z radiosonde runs made at Jamaica, Trinidad, and Swan Island, were about 199.5°K and 16,000 meters respectively. If one assumes that the clouds radiated as blackbodies with their tops at a level where the air temperature was approximately equal to the channel 2 T_{BB} measurements, one concludes that the cloud top lay near the tropopause [3]. It was also suggested [3] that the much higher accompanying channel 1 T_{BB} measurements (corresponding to a higher effective radiating height) resulted from a combination of the usually strong temperature inversion above the tropical tropopause and a very moist stratosphere.

The radiance emerging from the top of the atmosphere and in the direction of the satellite to which a given radiometer channel responds, $\bar{N}$, may be calculated from the equation of radiative transfer

$$N = \int_{\lambda=0}^{\infty} B_\lambda\ (T_o)\ \phi_\lambda\ \tau_\lambda\ (u_o^*)\ d\lambda$$

$$+ \int_{\lambda=0}^{\infty} \int_{\tau_o}^{1} B\ (T(u^*))\phi_\lambda\ d\tau_\lambda\ (u^*)\ d\lambda \qquad (3)$$

where B_λ = Plank function

T = Temperature

ϕ_λ = Spectral response of the infrared sensor

τ_λ = Spectral beam transmissivity in the direction of the satellite

λ = Wavelength

u^* = Reduced path length of the optically active gas

Subscript "o" = Surface of clouds or of the ground, assumed to radiate as a blackbody at ambient temperature within the spectral region of interest

In our calculations transmissivities $\tau_\lambda = \tau_\lambda\ (L \cdot u^*)$ given by Elsasser [11] were used where L is the generalized absorption coefficient. To transform the actual distributions of gas, pressure, and temperature along a beam to the satellite to the equivalent "reduced path, u*" in a homogeneous atmosphere for which values of τ_λ are tabulated, we used the equation

$$u^* = \int_o^u \left(\frac{P}{P_{\hat{s}}}\right)^k \left(\frac{T_{\hat{s}}}{T}\right)^{1/2} du \qquad (4)$$

where P = Pressure

T = Temperature

k = Exponent expressing the degree to which pressure broadening and the overlapping of the wings of the individual lines is considered

u = Actual path length of the optically active gas along a beam in the direction of the satellite

Subscript "s" = Indicates standard conditions of pressure (1013.25 mb) and temperature (293°K) for which transmission data are tabulated

The distribution function of water vapor which we would like to know is the specific humidity q(h) as a function of height, h. The relationship between u and q(h) in differential form is given by

$$du = \frac{P(h)}{R_d\, T(h)} \cdot q(h) \cdot \frac{dh}{\cos\,\theta} \tag{5}$$

where P(h) = Pressure as a function of height

T(h) = Temperature as a function of height

R_d = Gas constant for dry air (the effect of water vapor on the atmospheric mean molecular weight is considered negligible)

θ = Zenith angle of the beam in the direction of the satellite assuming a plane - parallel atmosphere

h = Height above the earth

The integrations of equations (4 and 5) were carried out on an electronic computer, and the integrations of the transfer equation (3) were accomplished by means of Möller-type radiation charts [14].

Suppose that a cloud surface near the tropopause radiates as a blackbody at a known ambient temperature; consequently, B_o would be known in the equation

$$N = B_o \tau_o (u^*) + \int_{\tau_o}^{1} B(T(u^*))\, d\tau(u^*) \qquad (6)$$

where the spectral subscripts and the integration over the channel response function of equation (3) are omitted for clarity. Further, suppose a measurement, N, in the water vapor channel is made at a known zenith angle, θ. It is impossible with the information at hand to reclaim the function $T(u^*)$ or, by extension, the desired function $q(h)$; one can only hope to determine various combinations of the integral and of $\tau_o(u^*)$ which will satisfy equation (6) for the known values of B_o and of N. However, by assuming plausible profiles of temperature, pressure, and water vapor, and, therefore, knowing from equations (4) and (5) the functional relationship $u^* = f[T(h), P(h), q(h), \cos\theta]$, one should in principle be able to infer at least gross features about the upper air water vapor abundance over the storm clouds, viz., whether the air is very wet or very dry. In attempting to apply the method in practice, one might expect that a measurement of B_o can be obtained from the window channel 2. The assumption that the cloud top radiates as a blackbody at its ambient temperature is of critical importance and is discussed further in (d) below. Although of relatively small effect at high altitudes, corrections of the order of 1^oK due to absorption by ozone, water vapor, and carbon dioxide could theoretically be applied to the window channel measurement [21].

Radiative transfer calculations for the response characteristics of the water vapor and window channels listed in [18] were carried out for normal incidence, indicating that ΔT_{BB}

values of about 10°K would be expected for a saturated stratosphere over cloud tops at the tropopause radiating as blackbodies at ambient temperature, taking the pressure dependence exponent k = 1 as given by Elsasser [6] in equation (4). Specifically, the tropical temperature profile from the Handbook of Geophysics [9] was used, modified above 22 km by the low latitude model proposed by Nordberg and Stroud [20], and the water vapor content up to 21 km was assumed to be saturated with respect to ice. Above 21 km, a constant mixing ratio of 0.11 gm kg of water vapor was assumed. The tropopause temperature in this model was 193.2°K, occurring at 16.8 km. These results were in essential agreement with preliminary calculations made in [3]. Of course for a completely dry stratosphere the channel 1 T_{BB} measurement would be equal to the tropopause temperature, 193.2°K, assuming that the cloud tops at that level radiate as blackbodies at ambient temperature. In general, the maximum calculated T_{BB} of 10°K decreases as either the stratospheric water vapor content decreases from saturation or as the blackbody radiating (cloud) surface is lowered from the tropopause. For a given water vapor distribution the ΔT_{BB} decreases as the cloud top is lowered toward increasingly warmer layers until it reaches zero. A further lowering of the cloud top then results in the channel 2 T_{BB} value once again resuming its "normal" relationship, i.e., higher than the channel 1 T_{BB} measurement.

However, by no plausible combination of conditions could we calculate a T_{BB} as large as the 26.5°K (uncorrected) of Figure 16. A closer examination of the measured values in both channels 1 and 2 indicates that with applicable corrections the measured maximum value of ΔT_{BB} = 26.5°K can indeed be reduced to

a value comparable to the 10°K required by the theory. The causes for such a correction are discussed in item (a) below. However, this method has not yet succeeded in practice to yield meaningful inferences of stratospheric water vapor content due to a number of complicating factors. Some of these factors have been resolved, at least in part, but others require further work before the method can be subjected to a valid test. We shall discuss briefly these factors below in items (b) through (e).

(a) Errors in the Calibration

The calibration must be accurate in absolute terms because of the requirements of determining accurately the effective radiating height of the cloud tops by means of channel 2 and of determining accurately the small difference, ΔT_{BB}, between two relatively large numbers. The estimated accuracy of the experiment as determined by the calibration is $\pm 5°K$ and $\pm 4°K$ for channels 1 and 2 respectively. But any changes in instrumental response after the original calibration, while they may not be of prime importance for such applications as the contour mapping of weather systems (cf. Figures 1-13), will seriously affect applications of the data where absolute measurements are required. Like the two solar radiation channels discussed above, the response of each of the infrared radiation channels was also observed to degrade as time passed. By observing the stability of the "space viewed (zero reference)" levels and by analyzing large masses of data statistically using the earth itself as a "calibration target", it was possible to develop degradation models for each channel and, hence, estimate corrections as a function of time. These corrections attempt to restore the telemetered data to absolute measurements.

It is emphasized, however, that the corrections are only simplified attempts at correcting empirically for several complicated degradation mechanisms which are not yet fully understood. The estimated corrections - additive for channel 2 and subtractive for channel 1 (~~viewing through the floor side~~) - are shown beside their respective calibrated equivalent blackbody temperatures in Figure 16. It is seen that after applying these corrections, the T_{BB} directly over the hurricane in Figure 16 decreases from 26.5°K to (223.5-8.5) - (197.0 + 3.7) = (215.0-200.7) = 14.3°K.

(b) System Noise

The spectral response of the water vapor channel is the narrowest of all the infrared channels and is situated in the short wavelength wings of the Planck distributions for temperatures observed in the atmosphere. Hence, channel 1 receives less radiant energy than channel 2, and its gain must be set much higher, thus decreasing its signal-to-noise ratio. This decreased signal-to-noise ratio is strikingly evident in Figure 16 where the error bars indicating the standard deviations, σ, are considerably larger for channel 1 than for channel 2. The standard deviations were determined by examining the fluctuations of the space viewed (zero reference) levels of both channels which ideally should be zero. One hundred and twenty-six values in equal time intervals were sampled in the space viewed portions in 8 consecutive scans over the hurricane and were subjected to statistical analysis. The resulting standard deviations were then applied to the radiation measurements over the hurricane. Unfortunately, the noise level of the data over the hurricane was greater by almost a factor of two

than the best quality data which have been obtained at other times in the TIROS system. It will be shown that if considerations of instrumental degradation and of reasonable statistical fluctuations (noise) are applied to channels 1 and 2, the resulting temperature difference ΔT_{BB} reduces to zero. For the degradation correction, the values obtained in (a) above were used. Considering noise, channel 1 measurements were arbitrarily reduced by 1.1σ and channel 2 measurements were increased by the same amount (Table II). A ΔT_{BB} of zero resulted which would infer a nearly dry stratosphere (assuming a blackbody cloud surface at a height below the tropopause corresponding to 206.3°K and assuming that the tropopause temperature is lower, a small amount of water vapor would be required in the stratosphere to counteract any water vapor in the region of the temperature minimum).

TABLE II

A Possible Modification of an Extreme Value of T_{BB} Considering Only System Noise and Instrumental Degradation

	T_{BB} (Calibrated values)	1.1 σ	T_{BB} (calibrated values altered by 1.1 σ	ST_{BB}	T_{BB} (Noise and Degradation Corrected)
Channel 1:	223.5°K	-4.8°K	218.7°K	-12.4°K	206.3°K
Channel 2:	197.0°K	+5.0°K	202.0°K	+4.3°K	206.3°K
ΔT_{BB} :	26.5°K		16.7°K		0

The application of a value of 1.1σ in opposite directions to channels 1 and 2 though realistic is rather arbitrary. The magnitude of the ΔT_{BB} values over the hurricane is, therefore, investigated further statistically. A scatter diagram of all pairs of T_{BB} measurements having nadir angles less than 40° (which corresponds to zenith angles less than 46°) was plotted from a computer listing of the eight swaths centered over the hurricane (Figure 17). A linear regression line was fitted by least squares and boundaries were drawn at a distance of 2 standard deviations (cf. Figure 16) in the channel 1 T_{BB} measurements above and below the regression line. A short dashed line marks the boundary along which the T_{BB} measurements of both channels are equal (after making degradation corrections). Figure 17 shows that even after correcting for degradation and considering noise, the linear regression line between channel 1 and channel 2 temperatures intersects the $\Delta T_{BB} = 0$ line at a value (215.7) which is appreciably larger than the assumed tropopause temperature. This would still imply a rather wet stratosphere. This conclusion, however, depends very critically upon the intersection between these two curves. The nature of the scatter in Figure 17 and the validity of fitting a linear regression line shall, therefore, be examined in greater detail.

A further investigation of Figure 17 indicates that only 84% of all points fall within the 2σ range shown by the dashed lines while theoretically one would expect 95% of all points to be within this range. This implies that a mechanism in addition to the system noise considered above, may contribute to the scattering. One such mechanism would be the incongruity between the fields of view of channel 1 and 2 which will be

discussed in (c) below. An additional factor contributing to the scatter can be attributed to inhomogeneities in the instantaneous intensity field viewed by the sensors. For example, if a channel 2 T_{BB} measurement of 235°K resulted from a high cold cloud filling part and a warm surface through clear skies filling the remainder of the 5° field of view, the corresponding channel 1 T_{BB} measurement would be lower than it would be if the 235°K channel 2 measurement resulted from a uniform cloud surface filling its field of view. Another contributing factor to the scatter in Figure 17 is limb darkening as the sensor nadir angles varied from 9° to 40°. However, the limb darkening effect was calculated to be less than 2°K. Another contributing factor to the scatter in Figure 17 could be a departure from horizontal water vapor stratification over the area swept by the scans. Such departures are to be expected in the lower atmosphere, but even high altitude water vapor has been observed to occur in concentration centers [16]. All these factors make the conclusion of a wet stratosphere based on Figure 17 rather tentative.

(c) Disparities in the Coordination of Measurements by Two Channels

In attempting to co mpare the measurements made by two different channels over a highly unstratified region such as that presented by the tops of storm clouds (cf. Figure 16), any differences in the time or spatial response coordinates of the measurements must be known, and corrections for them (if indeed possible) should be made. In the automatic processing of the radiation data each channel in a set of "simultaneous" measurements is actually sampled 0.0025 seconds after its predecessor in numerical order. However, a 0.0025 second sampling time

disparity between channel 1 and channel 2 is not appreciable where it takes about one sampling interval of 0.1309 seconds for the radiometer to rotate completely through one instantaneous field-of-view. Of far greater importance is the disparity which may exist between the response fields of the two channels (Figure 18). Laboratory field-of-view measurements indicate that, as a result of a slight misalignment, up to 0.15 of the instantaneous response field of channel 1 may lie outside the response field of channel 2 and vice versa. For example, if the observed channel 1 T_{BB} measurement at "A" in Figure 17 resulted from viewing an equivalent blackbody target of 216°K (degradation corrected) by 0.85 of the response field and an equivalent blackbody target of 233°K by 0.15 of the response field due to relative misalignment, the measurement, but for the misalignment, would have been at the tip of the arrow where the remaining deviation from 216°K could readily be attributed to noise alone. Similarly, if the observed channel 2 T_{BB} measurement at "B" in Figure 17 resulted solely from viewing an equivalent blackbody target of 216°K by 0.85 of the response field and an equivalent blackbody target of 283°K by 0.15 of the response field due to relative misalignment, the measurement, but for the misalignment, would have been at the tip of the arrow, inside the 2σ noise boundary. Both of these examples illustrate an additional mechanism for explaining the scatter of measurement in Figure 17, and point up an important problem in attempting to compare measurements from two different channels. Unfortunately, the laboratory measurements are not sufficient to permit correction for the field-of-view disparities between the two channels.

(d) Nonblackness of Clouds

Thick clouds have generally been assumed to radiate as blackbodies in the infrared part of the spectrum. To depart from this assumption would severely complicate many problems involving radiative processes in the atmosphere and would require extensive theoretical investigations of multiple-scattering by large particles as well as concurrent laboratory and empirical investigations of the problem. Relatively little work has been done in this area to date, but several sources indicate that the effective emissivity of clouds may depart appreciably from 1 in the infrared part of the spectrum, especially in the window region [4,5,10]. Deirmendjian [5] concludes that a considerable portion of the incident radiation in the window regions is scattered by clouds, thereby contributing to the infrared sky background usually attributed to blackbody emission. Consider a hypothetical T_{BB} measurement by both channel 1 and channel 2 of 208.7°K (cf. Figure 17). If the emissivity of the cloud top were, say, 0.80 in the region 7.5-13.5 microns while remaining unity in the region 5.9-6.7 microns, the channel 2 T_{BB} measurement would correspond to a cloud top temperature of about 215.7°K. To infer upper air water vapor content from such measurements under the assumption of blackbody clouds would therefore be erroneous. We have observed several cases of temperature inversions over high clouds in middle latitudes where the channel 1 T_{BB} measurement is still about 7°K higher than the channel 2 T_{BB} measurement after considering (insofar as possible) the effects of (a), (b), and (c) above. The stratospheric temperature profiles at those latitudes are nearly isothermal and in fact decrease slightly above the tropopause to a height of about 20 km.

Thus the role of stratospheric water vapor in increasing the channel 1 T_{BB} measurements in these cases is ruled out -- in fact the drier the stratosphere up to about 20 km, the higher would be the channel 1 T_{BB} measurement.

(e) Radiative Transfer Calculations

In our initial calculations we used a value of k = 1 to account for the pressure dependence of equation (4). However, theory and observation are not in complete accord in the matter of the pressure dependence, and there is some uncertainty as to the actual law which should be used [14,13,11,22] especially at low stratospheric pressures and gas concentrations which lie outside the laboratory conditions under which measurements are usually made. Elsasser [6] gives k = 1 in equation (4). However, there is by no means universal agreement on the value of k. For example, Kondratiev [13] gives k = 0.5 and Howard, Burch and Williams [11] give k = 0.6 for a "weak fit" and k = 0.72 for a "strong fit" in the 6.3 micron water vapor band. The value of k is not of great importance if most of the absorption takes place at relatively high pressures in the troposphere, but it becomes of considerable importance if most of the absorption takes place at stratospheric pressures of less than 100 mb. For example, in the case described above for a saturated stratosphere a $\Delta T_{BB} = 10^{o}K$ was calculated using k = 1. A second calculation was made under identical conditions of temperature, pressure, and water vapor, but using k = 0.5. This calculation yielded a $\Delta T_{BB} = 23^{o}K$.

There is some doubt as to the validity of using the reduction equation (4) in the region under consideration. Throughout our calculations, we ignored the temperature dependence of the absorption line intensities and assumed that atmospheric aerosols

played no part in the transfer of radiation.

Without attempting at this time to probe further into such questions as the theoretical aspects of the pressure and temperature dependencies, the validity of equation (4), the possible roles of other absorbers, and the question of scattering by clouds in the infrared, we shall merely state that a need for additional theoretical as well as experimental studies of radiative transfer at high altitudes is indicated before measurements in the lower stratosphere of the type discussed above can be interpreted with confidence.

7. Conclusions

The radiation maps of Hurricane Anna show that a severe storm of this type stands out clearly in all three of the infrared channels, and, in the daytime, also in the two solar channels of the TIROS medium resolution radiometer. The ability of the window and solar channels to track an intense storm system to a good degree of accuracy is demonstrated.

A detailed quantitative review of the ability of comparative measurements in the window and water vapor absorption channels to infer stratospheric water vapor content shows that the proposed method does not appear as promising as it did initially when the method was investigated qualitatively [3]. Although the principle of inferring stratospheric water vapor content over very high clouds remains valid, meaningful inferences at this time are precluded pending further investigations and work in at least five areas of uncertainty: namely systematic errors due to degradation of the instruments during flight, random errors due to noise in the telemetered signals, incongruities between the response fields of channels 1 and 2, nonvalidity of the assumption of the "blackness" of clouds in the atmospheric window, and the uncertainties of radiative transfer theory as it applied to our calculations.

ACKNOWLEDGEMENTS

We should like to express our thanks to Mr. Robert Hite, Goddard Space Flight Center, who carried out the reduction of the radiation data on an IBM 7090 computer, and to Mr. William Callicott, Meteorological Satellite Laboratory, U. S. Weather Bureau, who devised the mercator mapping program used to produce the maps shown in this paper.

REFERENCES

1. Annual Tropical Storm Report, 1961, U. S. Fleet Weather Facility, Miami, Florida. OPNAV Report 3140-9.

2. Bandeen, W. R., R. A. Hanel, John Licht, R. A. Stampfl, and W. G. Stroud, "Infrared and Reflected Solar Radiation Measurements from the TIROS II Meteorological Satellite". J. Geophys. Res., 65, 3169-3185, 1961.

3. Bandeen, W. R., B. J. Conrath, W. Nordberg, and H. P. Thompson, 1963, "A Radiation View of Hurricane Anna from the TIROS III Meteorological Satellite". pp. 224-233 in Proceedings of the First International Symposium on Rocket and Satellite Meteorology, Washington, D. C., April 23-25, 1962, ed. by H. Wexler and J. E. Caskey, Jr., North-Holland Publishing Company, Amsterdam.

4. Deirmendjian, D., "Scattering and Polarization Properties of Polydispersed Suspensions with Partial Absorption". Paper presented at Interdisciplinary Conference on Electromagnetic Scattering, Potsdam, N. Y., August 1962, published as memorandum RM-3228-PR, Contract No. AF 49(638)-700, The Rand Corporation, Santa Monica, Calif., July 1962.

5. Deirmendjian, D., "Atmospheric Extinction of Infrared Radiation". Quar. J. R. Meteor. Soc., 86, 371-381, 1962.

6. Elsasser, W. M., "Atmospheric Radiation Tables". Meteorological Monographs, Am. Meteor. Soc., Vol. 4, No. 23, August 1960.

7. Fritz, Sigmund and Jay S. Winston, "Synoptic Use of Radiation Measurements from Satellite TIROS II". Monthly Weather Review, 90, 1-9, 1962.

REFERENCES (Continued)

8. Hanel, R. A. and W. G. Stroud, "The TIROS II Radiation Experiment". Tellus XIII, 484-488, 1961.

9. Hanel, R. A. and D. Q. Wark, "TIROS II Radiation Experiment and Its Physical Significance". J. Opt. Soc. Amer. 51, 1394-1399, 1961.

10. Handbook of Geophysics, (1960) Revised Edition, Air Research and Development Command, Air Force Research Division, Geophysics Research Directorate, The MacMillan Company, New York.

11. Havard, J. B., "On the Radiational Characteristics of Water Clouds at Infrared Wave Lengths", Ph.D. Thesis, Univ. of Wash., 1960.

12. Howard, J. N., D. L. Burch, and D. Williams, "Infrared Transmission through Synthetic Atmospheres". J. Opt. Soc. Am., 46, 242-245, 334-338, 1956 (Or "Near Infrared Transmission through Synthetic Atmospheres". Geophysical Research Papers No. 40, AFCRC-TR-55-213, Geophysics Research Directorate, AFCRC, Bedford, Mass., Nov. 1955.)

13. Kaplan, L. D., "On the Pressure Dependence of Radiative Heat Transfer in the Atmosphere". J. Meteor., 9, 1-12, 1952.

14. Kondratiev, K. Y. and H. I. Mulisk, "Comparison of Radiation Charts". Geofisica Pura E Applicata, 46, 231-240, 1960/II.

15. Möller, F., "Long Wave Radiation" in Compendium of Meteorology, edited by Thomas F. Malone, Am. Meteor. Soc., Boston, 1951.

16. Möller, Fritz, "Some Preliminary Evaluations of TIROS II Radiation Measurements". Archiv fur Meteorologie, Geophysik und Bioklimatologie, 12, Series B, No. 1, pp. 78-94, July 1962.

REFERENCES (Continued)

17. Murcray, D. G., F. H. Murcray, and W. J. Williams, "Distribution of Water Vapor in the Stratosphere as Determined from Infrared Absorption Measurements". J. Geophys. Research, 67, 759-766, 1962.

18. Nordberg, W., W. R. Bandeen, B. J. Conrath, V. Kunde and I. Persano, "Preliminary Results of Radiation Measurements from the TIROS III Meteorological Satellite". J. Atmos. Sci., 19, 20-30, 1962.

19. Staff members of the Aeronomy and Meteorology Division, Goddard Space Flight Center, "TIROS III Radiation Data Users' Manual". Goddard Space Flight Center, NASA, Greenbelt, Maryland, August 1962, 17 pp.

20. Staff members of the Aeronomy and Meteorology Division, Goddard Space Flight Center, and of the Meteorological Satellite Laboratory, U. S. Weather Bureau, "TIROS III Radiation Data Catalog". Goddard Space Flight Center, NASA, Greenbelt, Maryland, December 1962, 388 pp.

21. Stroud, W. G. and W. Nordberg, "Seasonal, Latitudinal, and Diurnal Variations in the Upper Atmospheres". NASA Technical Note D-703, Goddard Space Flight Center, Greenbelt, Maryland, 1961.

22. Wark, D. Q., G. Yamamoto, and J. H. Lienesch, "Methods of Estimating Infrared Flex and Surface Temperature from Meteorological Satellites". J. Atmos. Sci., 19, 369-384, Sept. 1962.

FIGURES

Figure 1 - Radiation map: channel 1 (5.9-6.7 microns), orbit 132, 21 July 1961, 1545 GMT - 1602 GMT. Hurricane Anna is centered near latitude 13.8°N, longitude 72.3°W. Original grid scale: 2.5 degrees of longitude per mesh interval.

Figure 2a- Radiation map: channel 2 (7.5-13.5 microns). Original grid scale: 2.5 degrees per mesh interval. (cf. Fig. 1)

Figure 2b- Radiation map: channel 2 (7.5-13.5 microns). Original grid scale: 1.25 degrees per mesh interval. (cf. Fig. 1)

Figure 3 - Radiation map: channel 3 (0.2-7.0 microns). Original grid scale: 2.5 degrees per mesh interval. (cf. Fig. 1)

Figure 4 - Radiation map: channel 4 (7.0-32.0 microns). Original grid scale: 2.5 degrees per mesh interval. (cf. Fig. 1)

Figure 5 - Radiation map: channel 5 (0.5-0.75 microns). Original grid scale: 2.5 degrees per mesh interval. (cf. Fig. 1)

Figure 6 - Composite radiation map: channel 2 (7.5-13.5 microns), orbits 89 and 90, 18 July 1961. The incipient Hurricane Anna is centered near latitude 12.0°N, longitude 49.0°W. Original grid scale: 2.5 degrees of longitude per mesh interval.

Figure 7 - Composite radiation map: channel 5 (0.5-0.75 microns). (cf. Fig. 6)

Figure 8 - Composite radiation map: channel 2 (7.5-13.5 microns), orbits 102, 103, and 104, 19 July 1961. The incipient Hurricane Anna is centered near latitude 11.0°N, longitude 58.0°W. Original grid scale: 2.5 degrees of longitude per mesh interval.

Figure 9 - Composite radiation map: channel 5 (0.5-0.75 microns), (cf. Fig. 8)

Figure 10 - Composite radiation map: channel 2 (7.5-13.5 microns), orbits 117 and 118, 20 July 1961. Hurricane Anna is centered near latitude 11.5°N, longitude 65.5°W. Original grid scale: 2.5 degrees of longitude per mesh interval.

Figure 11 - Composite radiation map: channel 5 (0.5-0.75 microns). (cf. Fig. 10)

Figure 12 - Composite radiation map: channel 2 (7.5-13.5 microns), orbits 174 and 175,24 July 1961. The dissipating Hurricane Anna is centered near latitude 17.5°N, longitude 89.0°W. Original grid scale: 2.5 degrees of longitude per mesh interval.

Figure 13 - Composite radiation map: channel 5 (0.5-0.75 microns). (cf. Fig. 12)

Figure 14 - Television picture taken by TIROS III, orbit 132, 21 July 1961, 1549:50 GMT. Hurricane Anna is the upper cloud mass, centered about 70 miles north of the Guajira Peninsula of Colombia. The Colombian coast runs horizontally to the west and joins Panama (near the upper left fiducial mark). Lake Maracaibo is cradled in the upper right-hand quadrant of the central fiducial cross.

Figure 15 - Television picture taken by TIROS III, orbit 132, 21 July 1961, 1552:20 GMT. The cloud mass which is south of Hurricane Anna is seen at the top of the picture. The central fiducial cross is near the headwaters of the Orinoco River in southern Venezeula. The lower portion of the photograph reveals the scattered-to-clear condition over the Amazon region of Brazil.

Figure 16 - Superimposed analog signals of the 5.9-6.7 micron water vapor channel 1 and the 7.5-13.5 micron window channel 2 from one swath over Hurricane Anna. Time increases to the right along the abscissa, extending 6.446 seconds, the period of one satellite rotation. The ordinates show originally calibrated equivalent blackbody temperatures, T_{BB}, and estimated corrections, ST_{BB}, to be applied during orbit 132 for, respectively, channel 2 on the left and channel 1 on the right. The error bars, drawn where the sensors were looking directly over the hurricane, indicate one standard deviation of the analog signals. 0.1309 seconds is the sampling period normally employed in automatic data processing.

Figure 17 - Scatter diagram of equivalent blackbody temperatures, T_{BB}, measured by channels 1 and 2 during eight swaths over Hurricane Anna. Estimated corrected values of T_{BB} are shown in parentheses by the originally calibrated values. Only measurements having sensor nadir angles less than 40^{o} are plotted. The solid linear regression line was fitted by least squares. The dashed boundaries are displaced from the regression line by the equivalent of two standard deviations (cf. Figure 16) in the channel 1 measurements.

Figure 18 - Schematic of response fields deduced from laboratory measurements, illustrating the relative misalignment between channels 1 and 2. The response in any direction is given in cylindrical coordinates (θ, φ, Z) where θ and φ are, respectively, the radial and tangential direction angles and Z the corresponding response level. The sensor optical axis is coincident with the Z axis. The laboratory measurements determine a response (Z) for the incremental solid angle in every direction (θ,φ). The loci of all points $p = p(\theta,\varphi,Z)$ describe the response fields (or "response surfaces"). The relative response levels in two specific directions are illustrated.

TIROS III SCANNING RADIOMETER

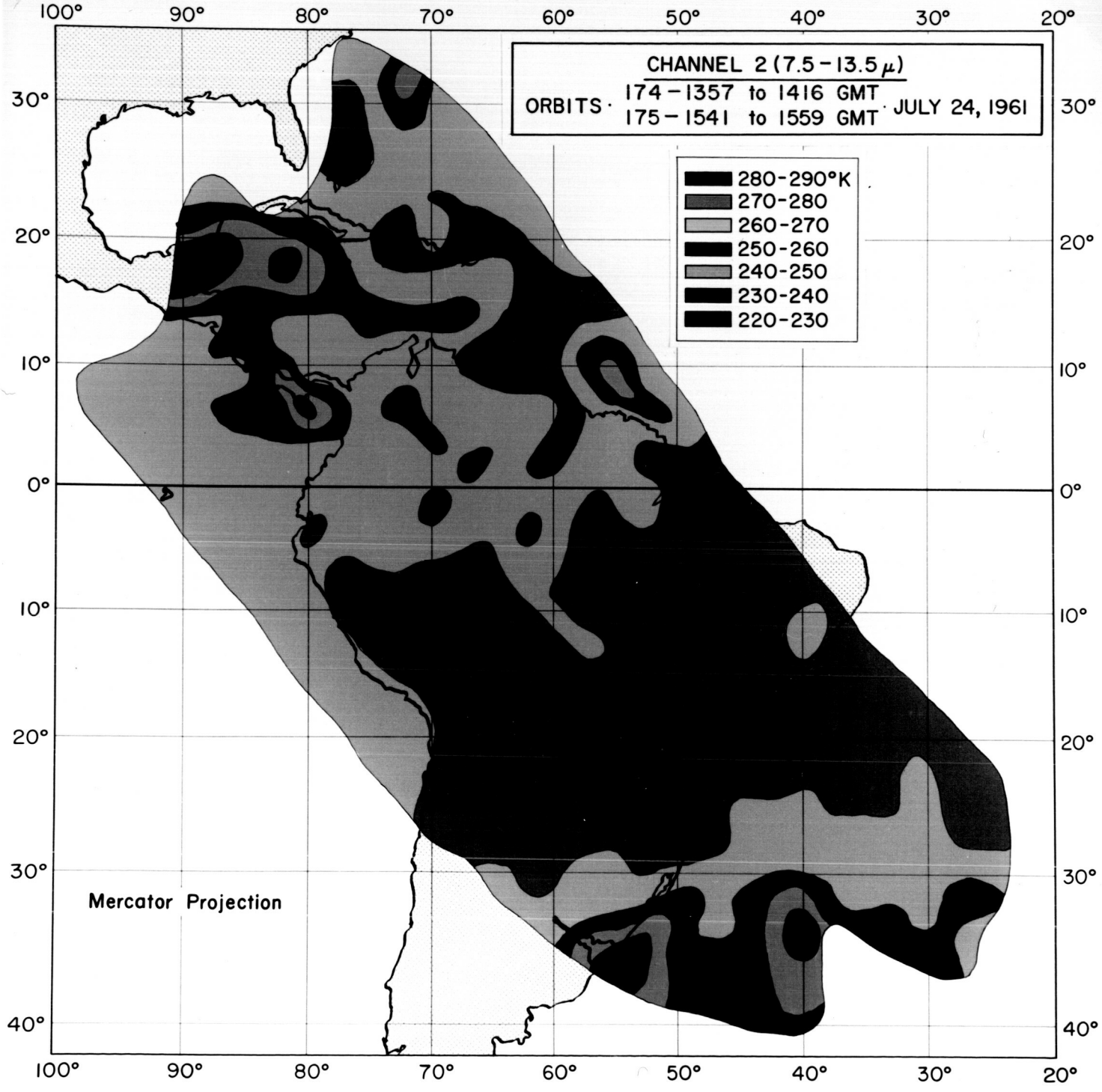

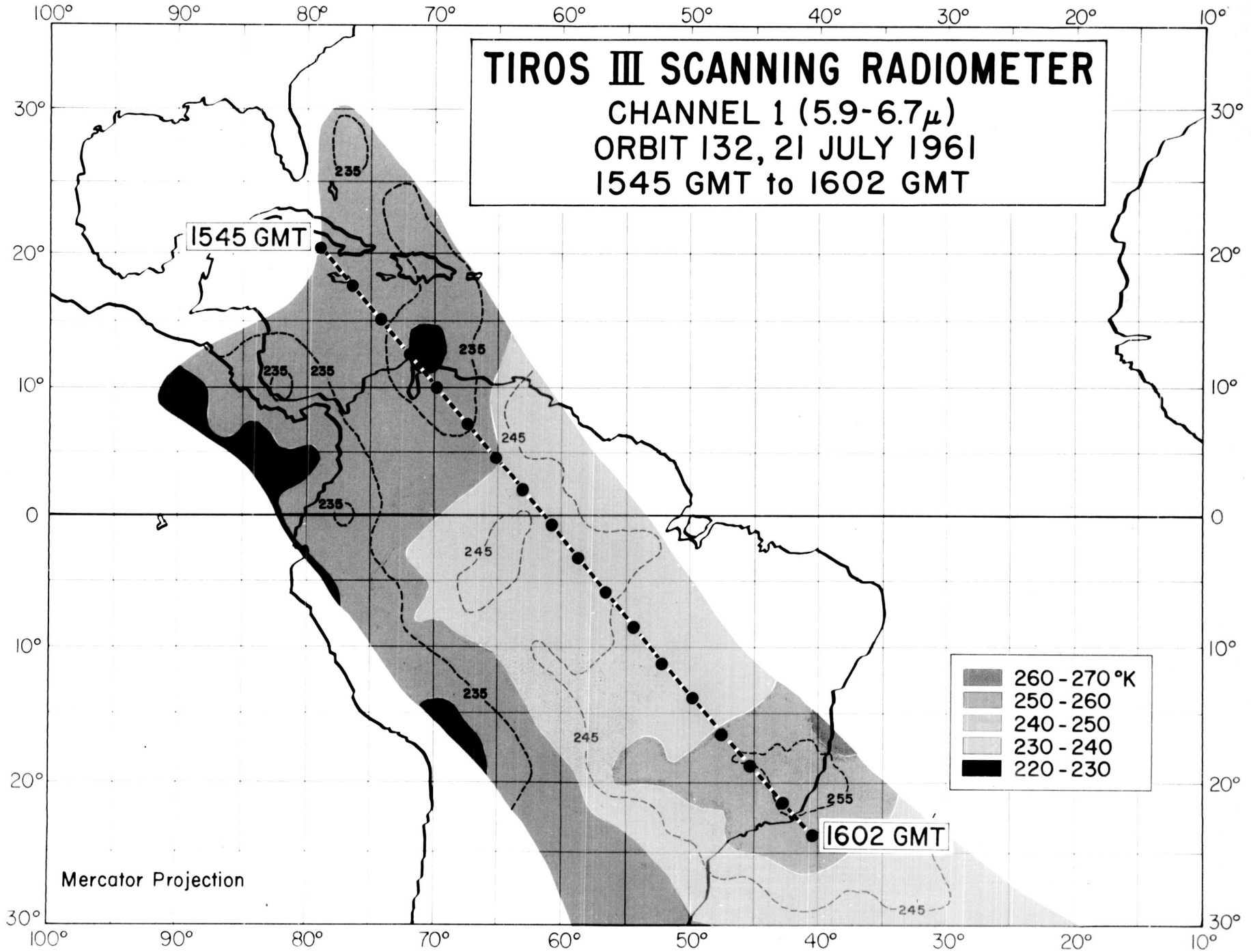
TIROS III SCANNING RADIOMETER
CHANNEL 1 (5.9-6.7μ)
ORBIT 132, 21 JULY 1961
1545 GMT to 1602 GMT
1545 GMT
1602 GMT
260 - 270 °K
250 - 260
240 - 250
230 - 240
220 - 230
235
245
255
Mercator Projection
100°
90°
80°
70°
60°
50°
40°
30°
20°
10°
30°
20°
10°
0
10°
20°
30°

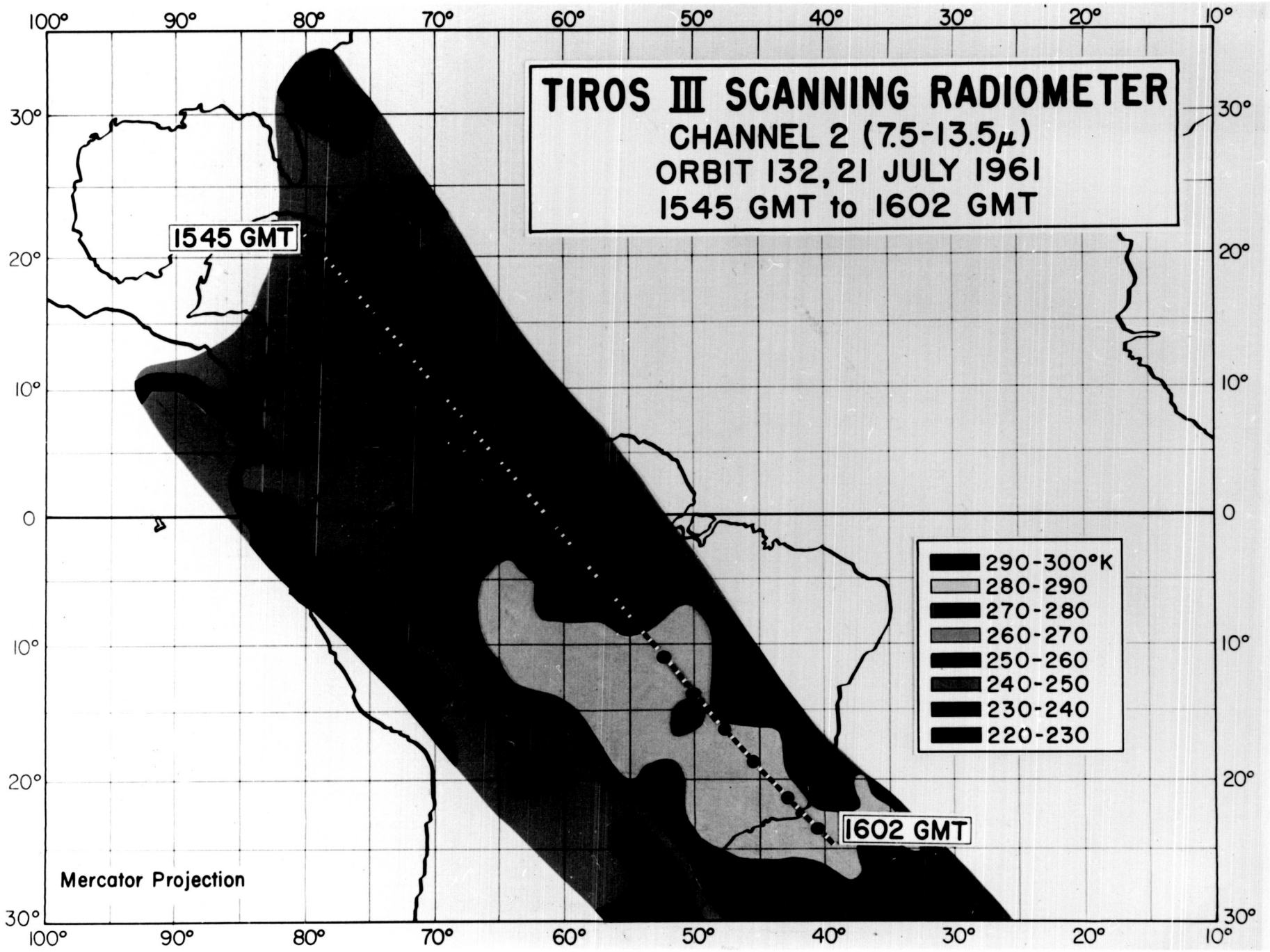
TIROS III SCANNING RADIOMETER
CHANNEL 2 (7.5-13.5μ)
ORBIT 132, 21 JULY 1961
1545 GMT to 1602 GMT
1545 GMT
1602 GMT
290-300°K
280-290
270-280
260-270
250-260
240-250
230-240
220-230
Mercator Projection
100°
90°
80°
70°
60°
50°
40°
30°
20°
10°
30°
20°
10°
0
10°
20°
30°

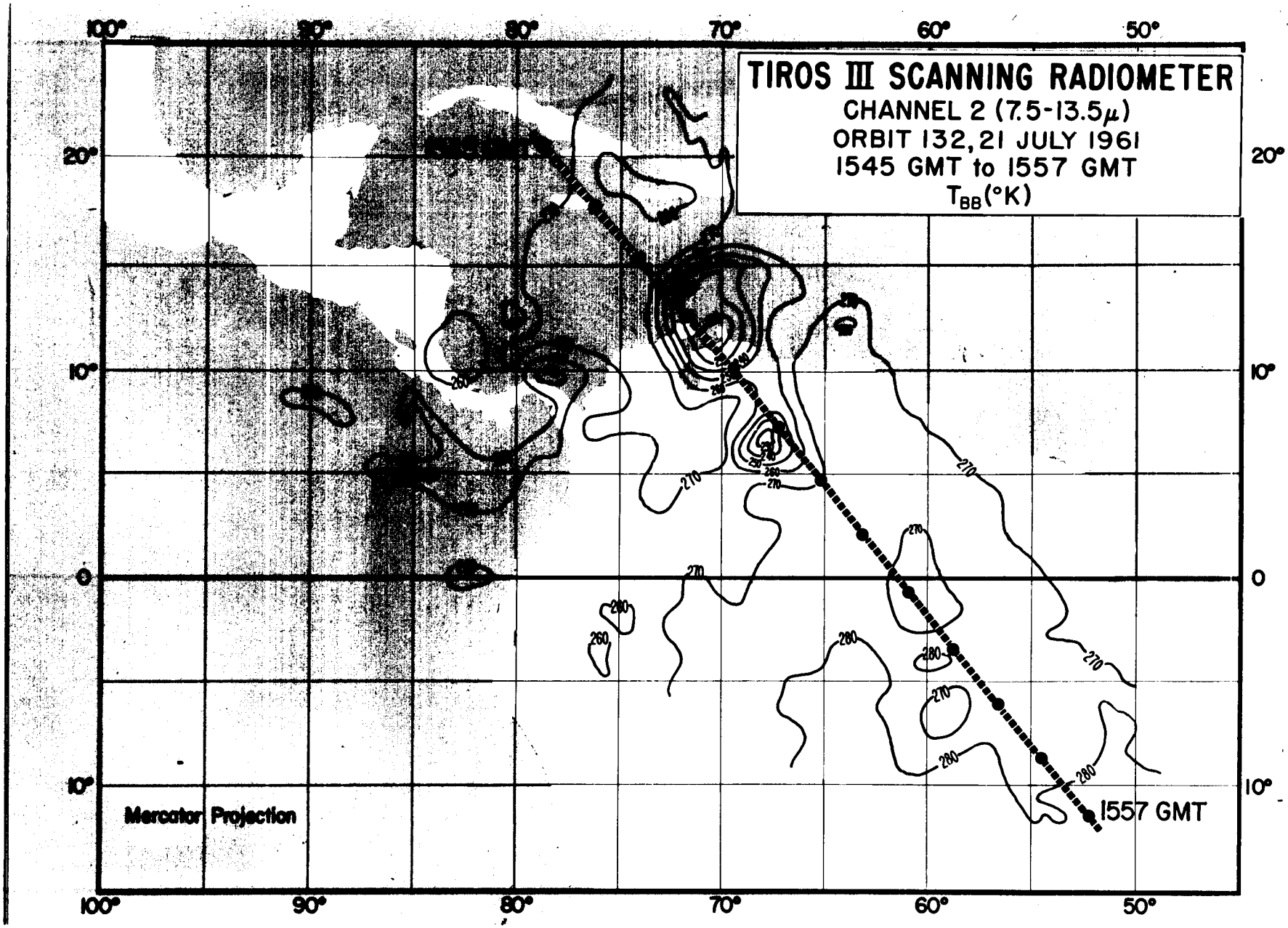
TIROS III SCANNING RADIOMETER
CHANNEL 2 (7.5-13.5μ)
ORBIT 132, 21 JULY 1961
1545 GMT to 1557 GMT
T_{BB}(°K)
100°
90°
80°
70°
60°
50°
20°
10°
0
10°
260
270
280
1557 GMT
Mercator Projection

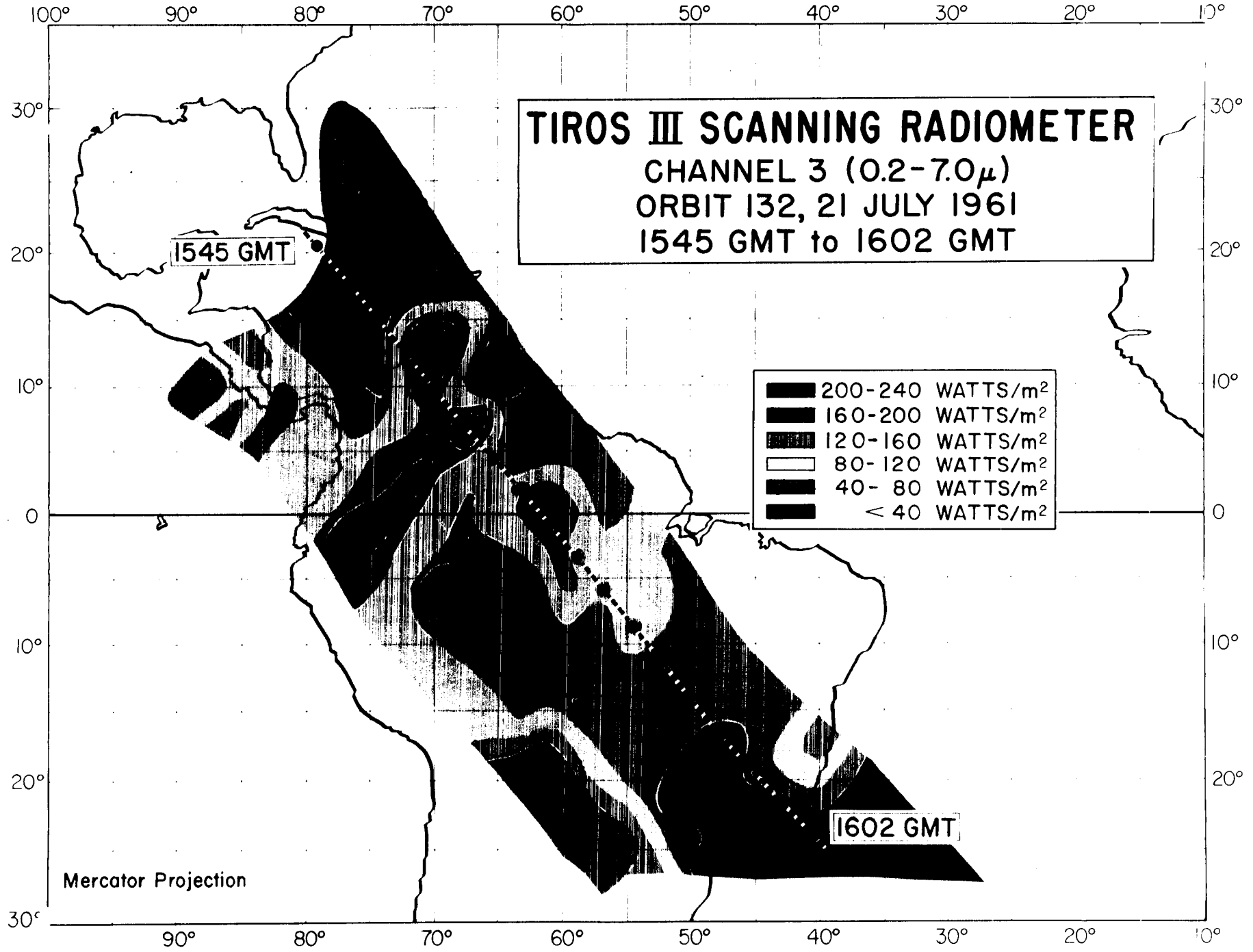
TIROS III SCANNING RADIOMETER
CHANNEL 3 (0.2-7.0μ)
ORBIT 132, 21 JULY 1961
1545 GMT to 1602 GMT
1545 GMT
1602 GMT
200-240 WATTS/m²
160-200 WATTS/m²
120-160 WATTS/m²
80-120 WATTS/m²
40-80 WATTS/m²
< 40 WATTS/m²
Mercator Projection
100° 90° 80° 70° 60° 50° 40° 30° 20° 10°
30° 20° 10° 0 10° 20° 30°

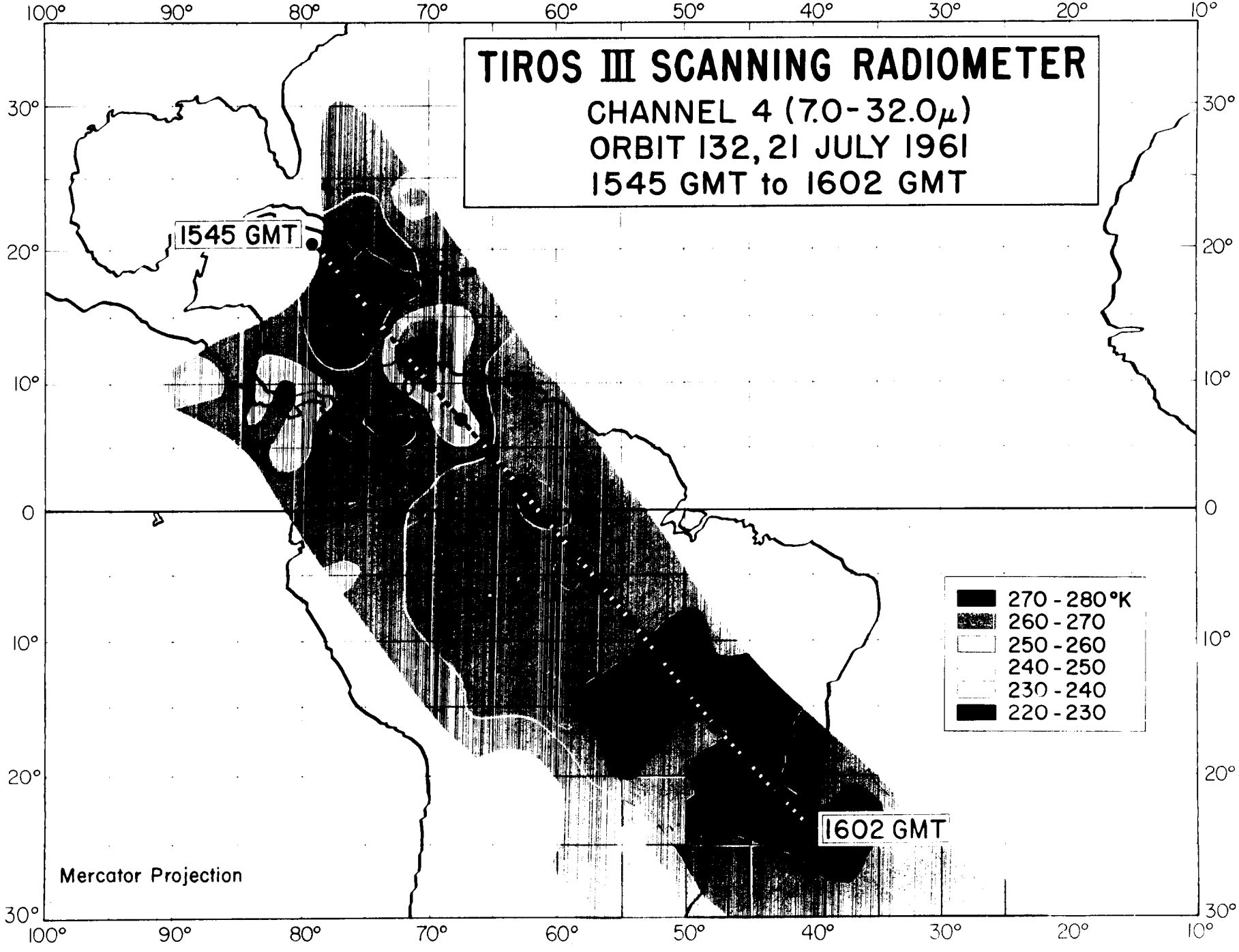
TIROS III SCANNING RADIOMETER
CHANNEL 4 (7.0-32.0μ)
ORBIT 132, 21 JULY 1961
1545 GMT to 1602 GMT
1545 GMT
1602 GMT
270 - 280°K
260 - 270
250 - 260
240 - 250
230 - 240
220 - 230
Mercator Projection
100°
90°
80°
70°
60°
50°
40°
30°
20°
10°
30°
20°
10°
0
10°
20°
30°

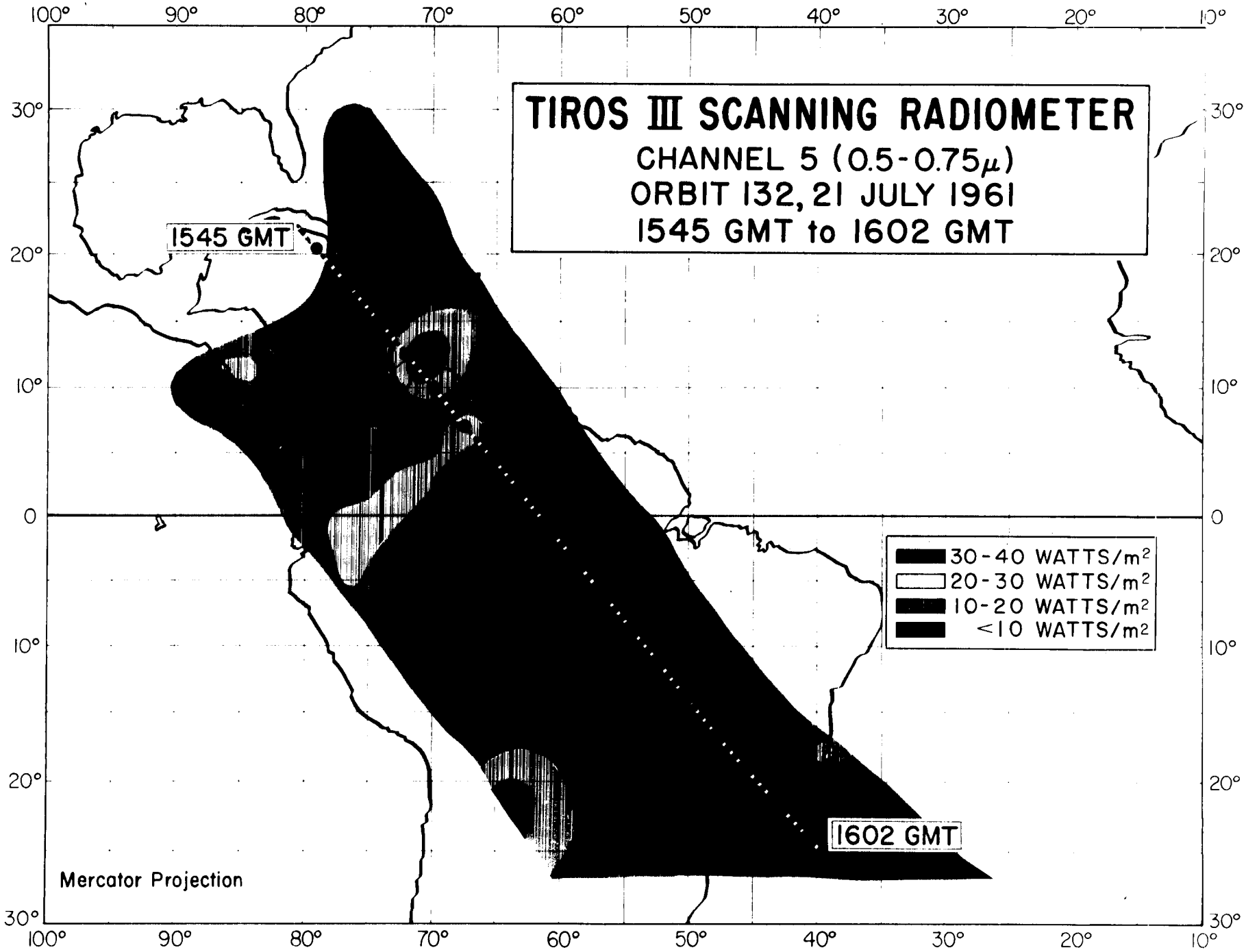
TIROS III SCANNING RADIOMETER
CHANNEL 5 (0.5-0.75μ)
ORBIT 132, 21 JULY 1961
1545 GMT to 1602 GMT
1545 GMT
1602 GMT
30-40 WATTS/m²
20-30 WATTS/m²
10-20 WATTS/m²
<10 WATTS/m²
Mercator Projection
100° 90° 80° 70° 60° 50° 40° 30° 20° 10°
30° 20° 10° 0 10° 20° 30°

TIROS III SCANNING RADIOMETER

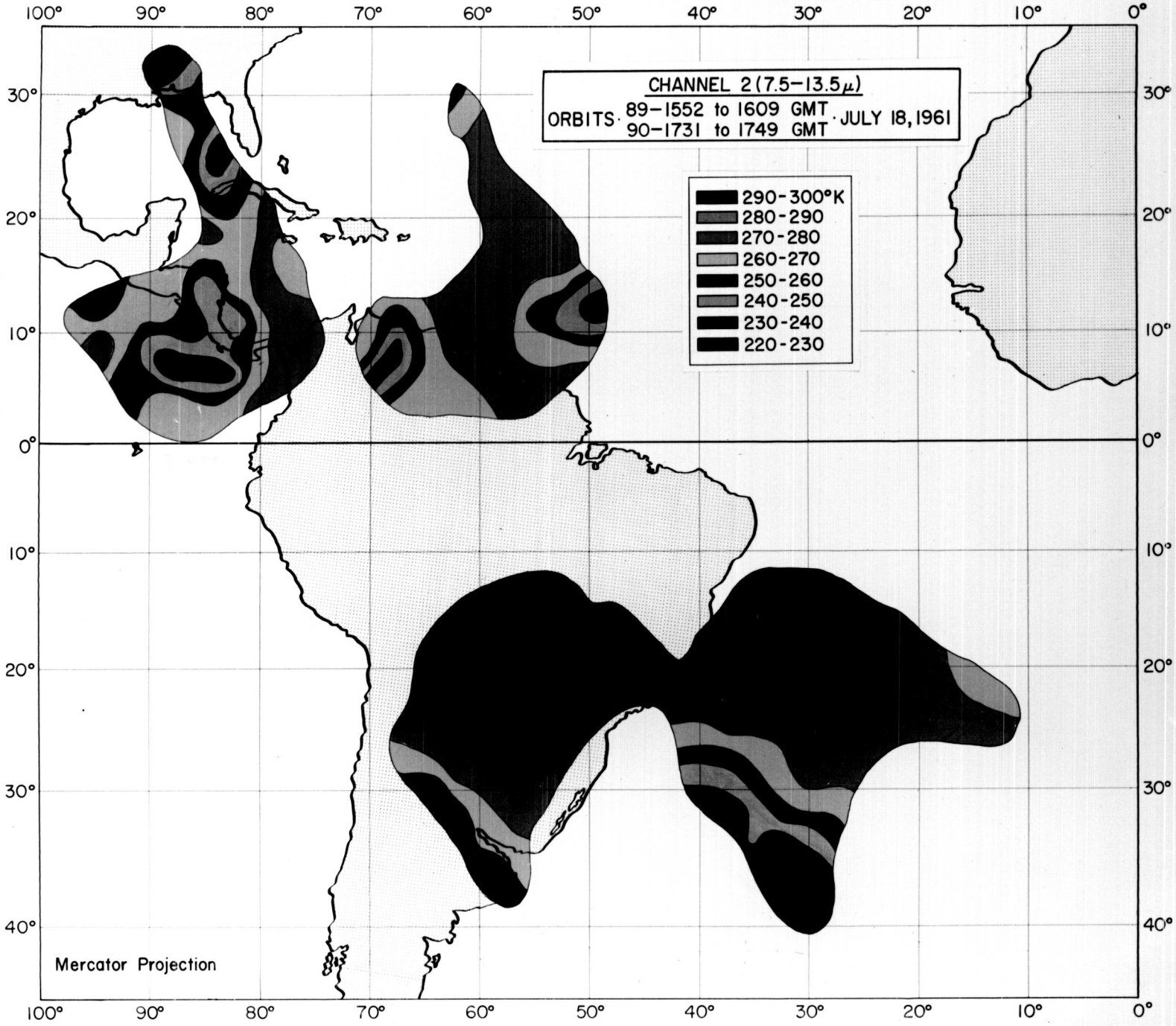

TIROS III SCANNING RADIOMETER

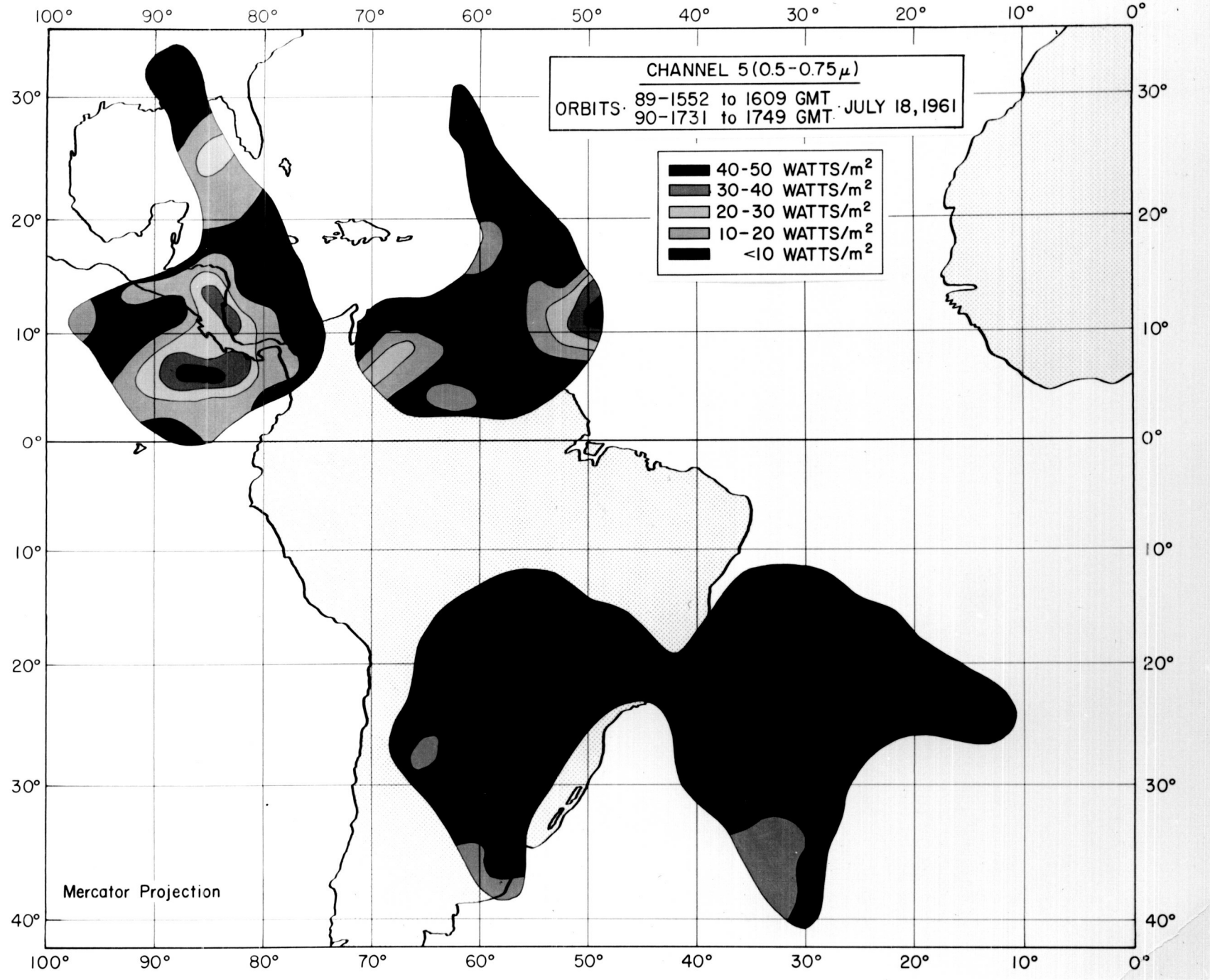

TIROS III SCANNING RADIOMETER

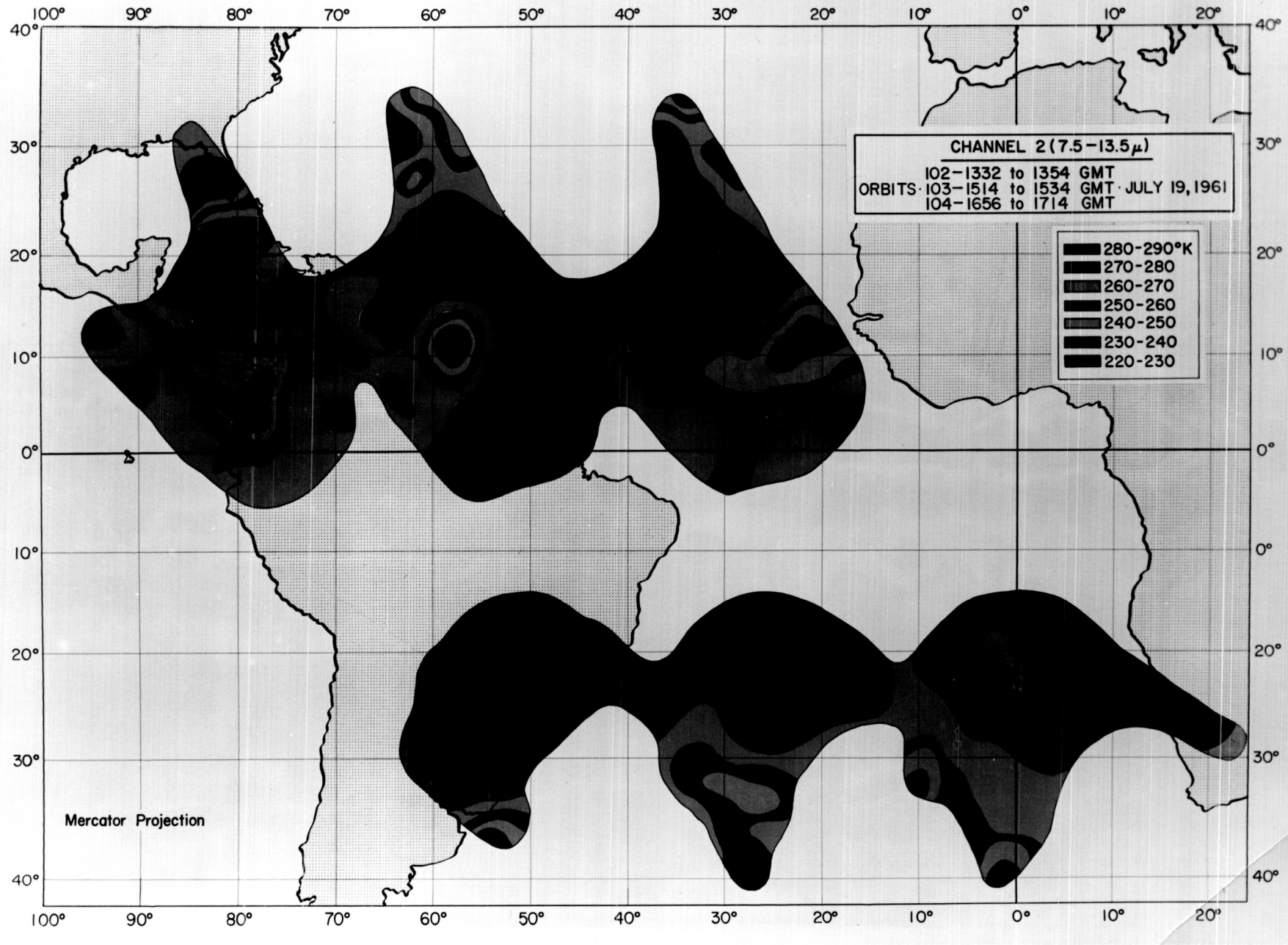

TIROS III SCANNING RADIOMETER

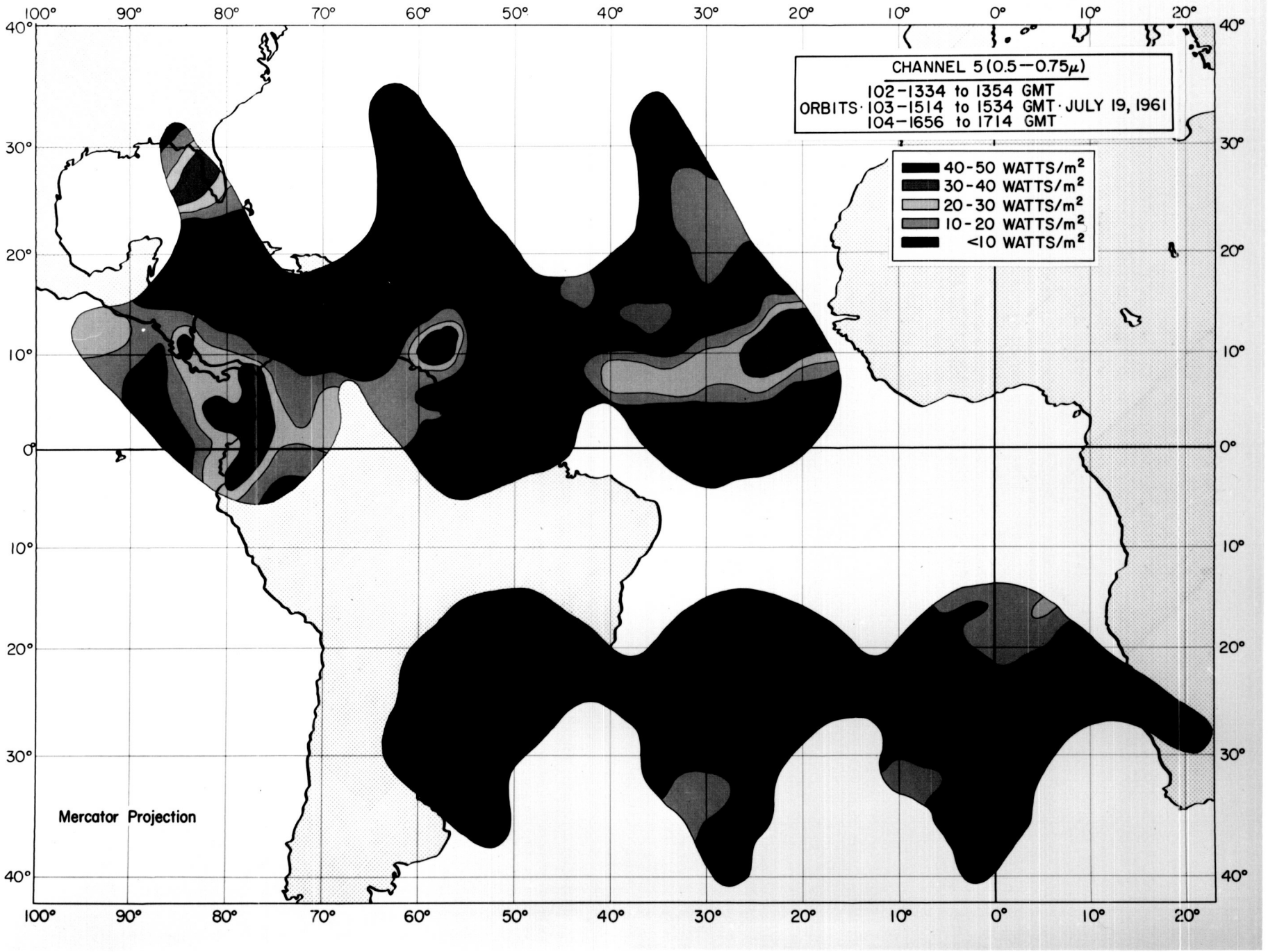

TIROS III SCANNING RADIOMETER

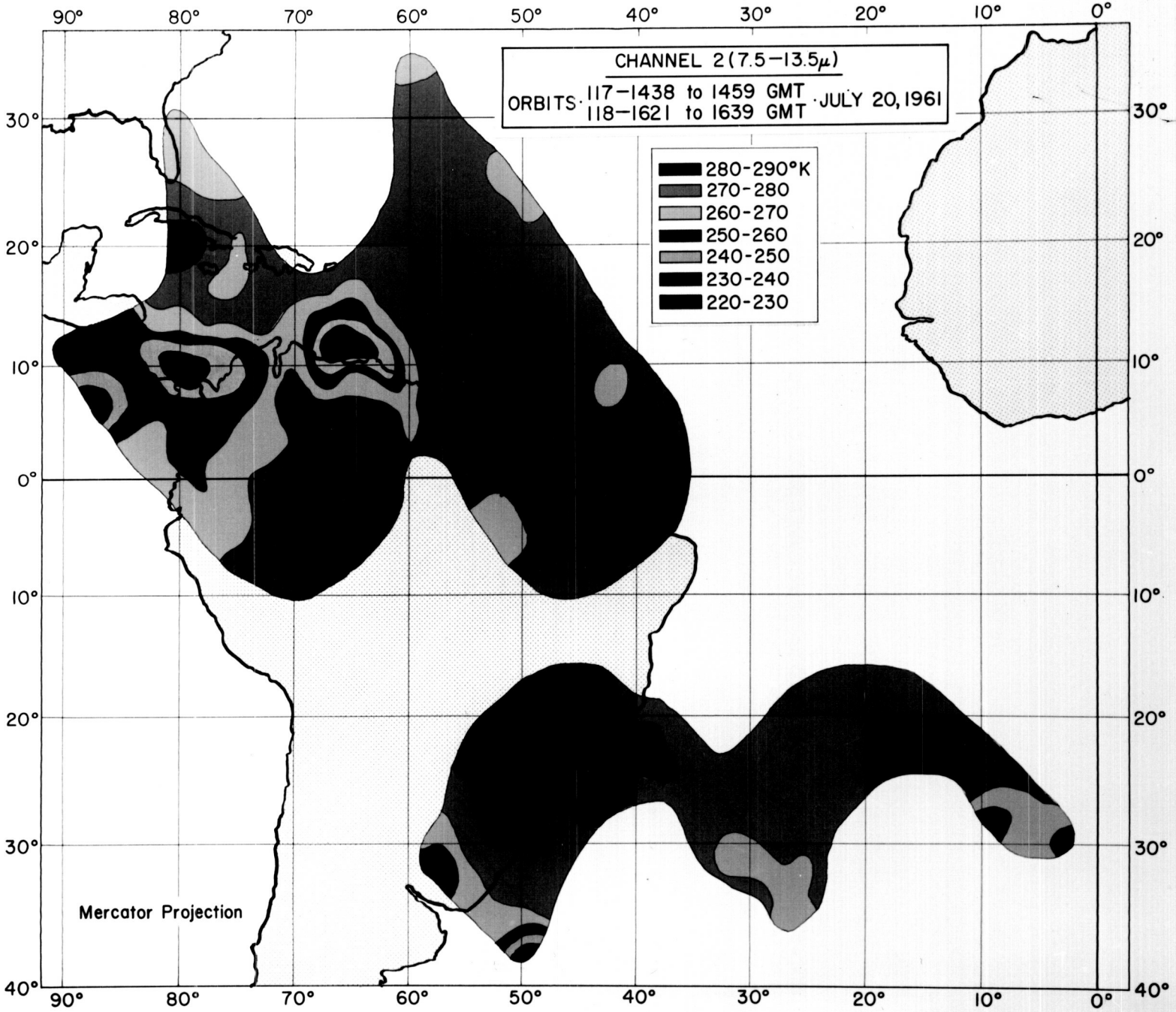

TIROS III SCANNING RADIOMETER

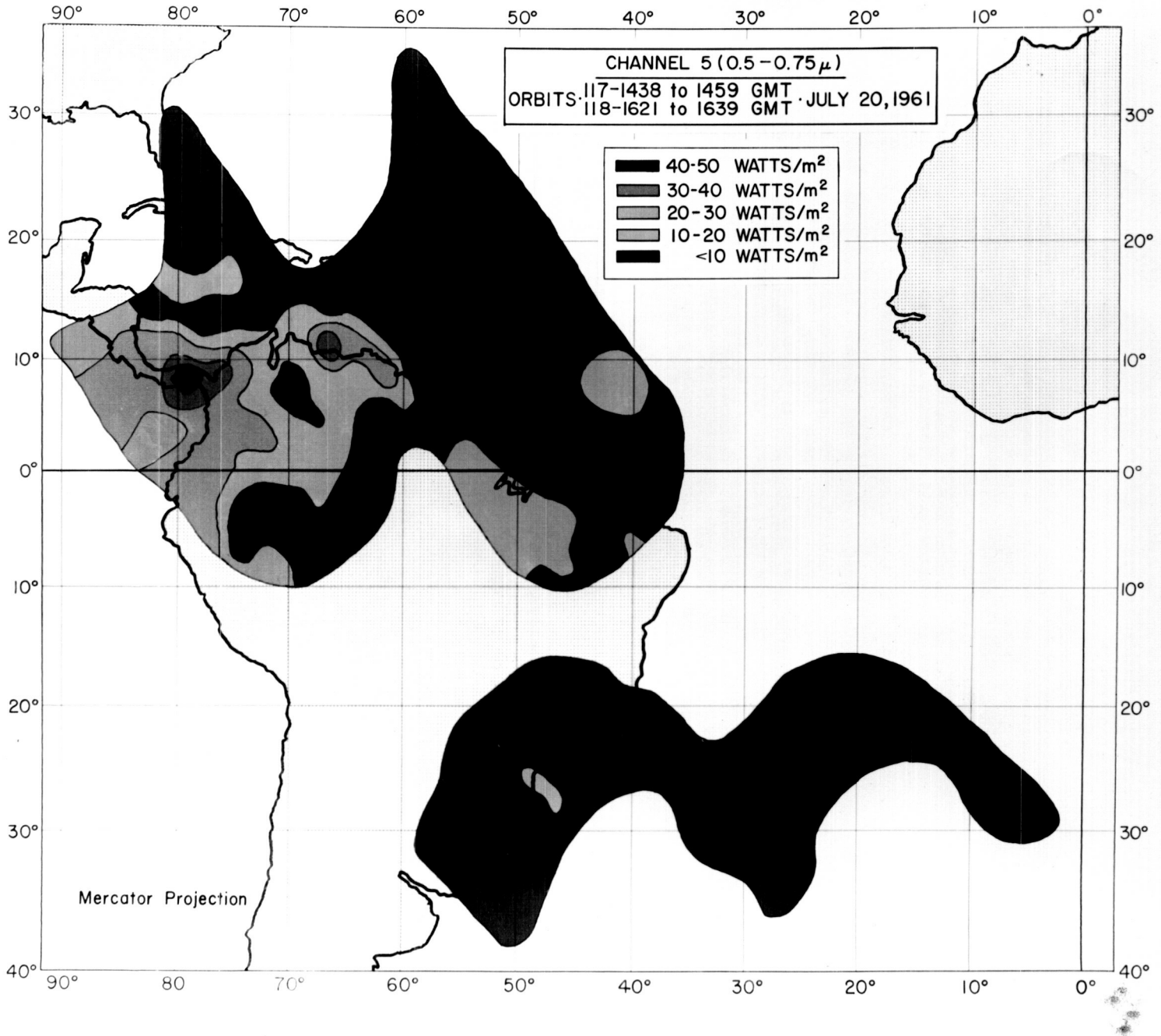

TIROS III SCANNING RADIOMETER

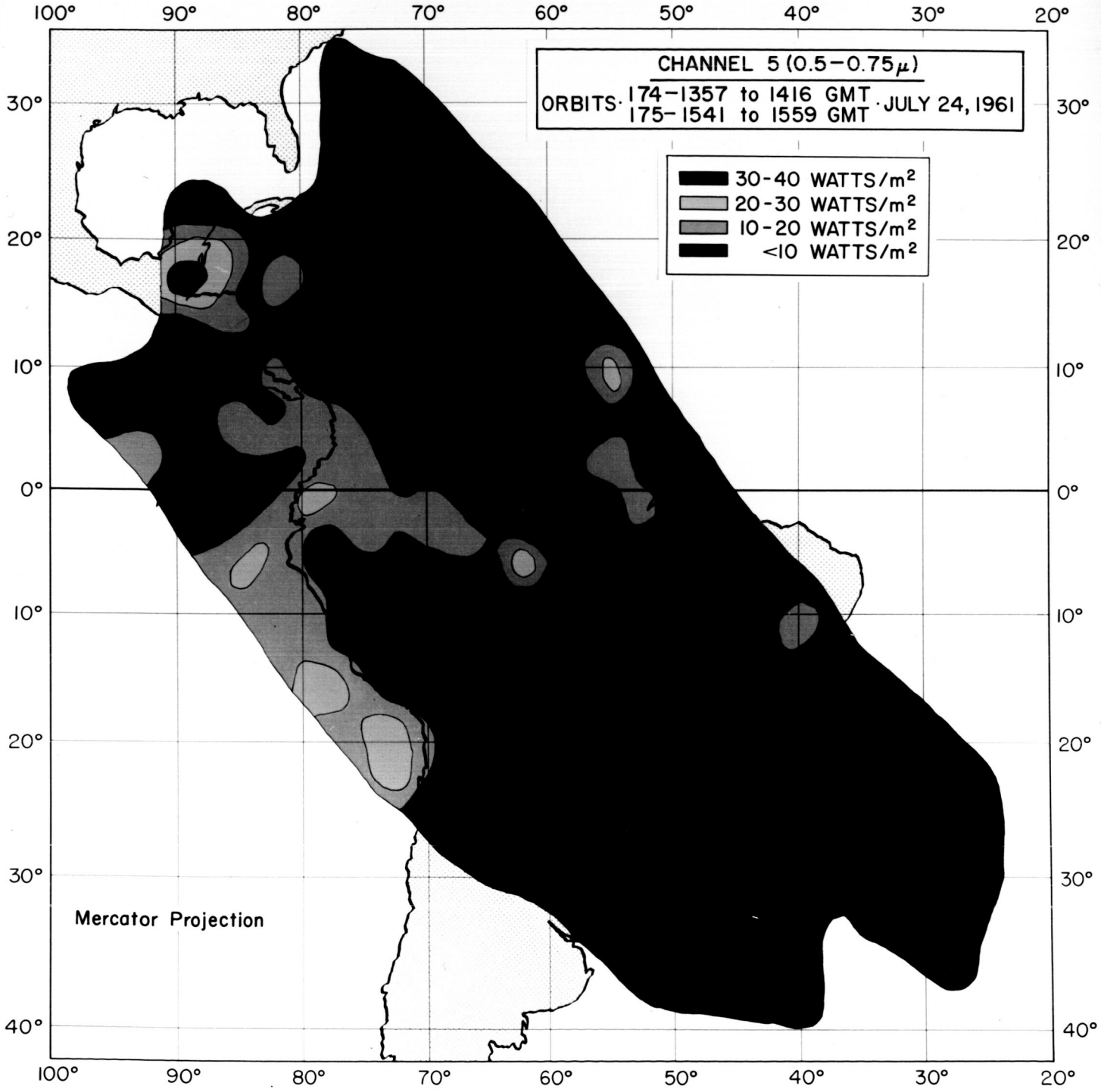

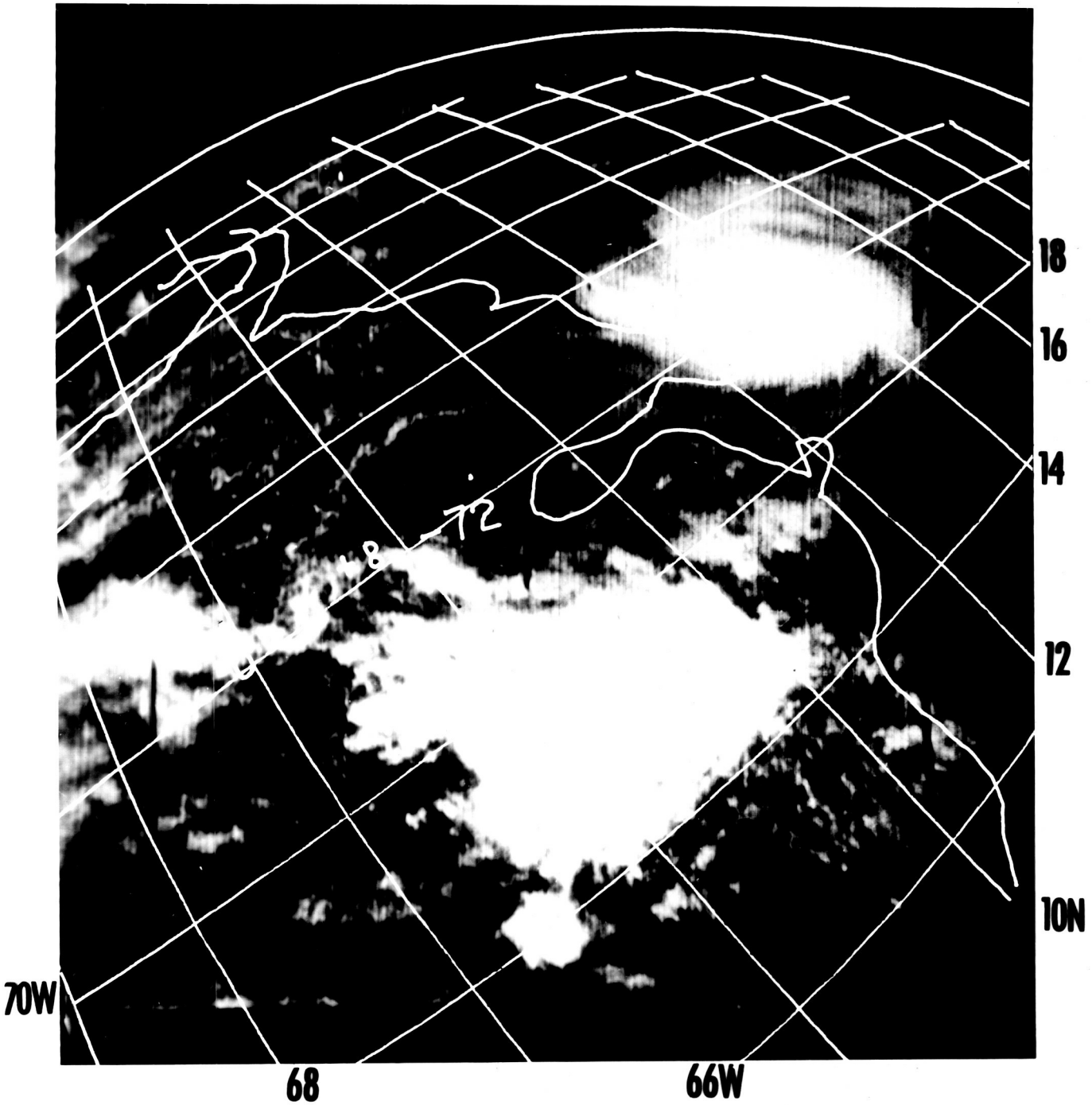
18
16
14
12
10N
70W
68
66W

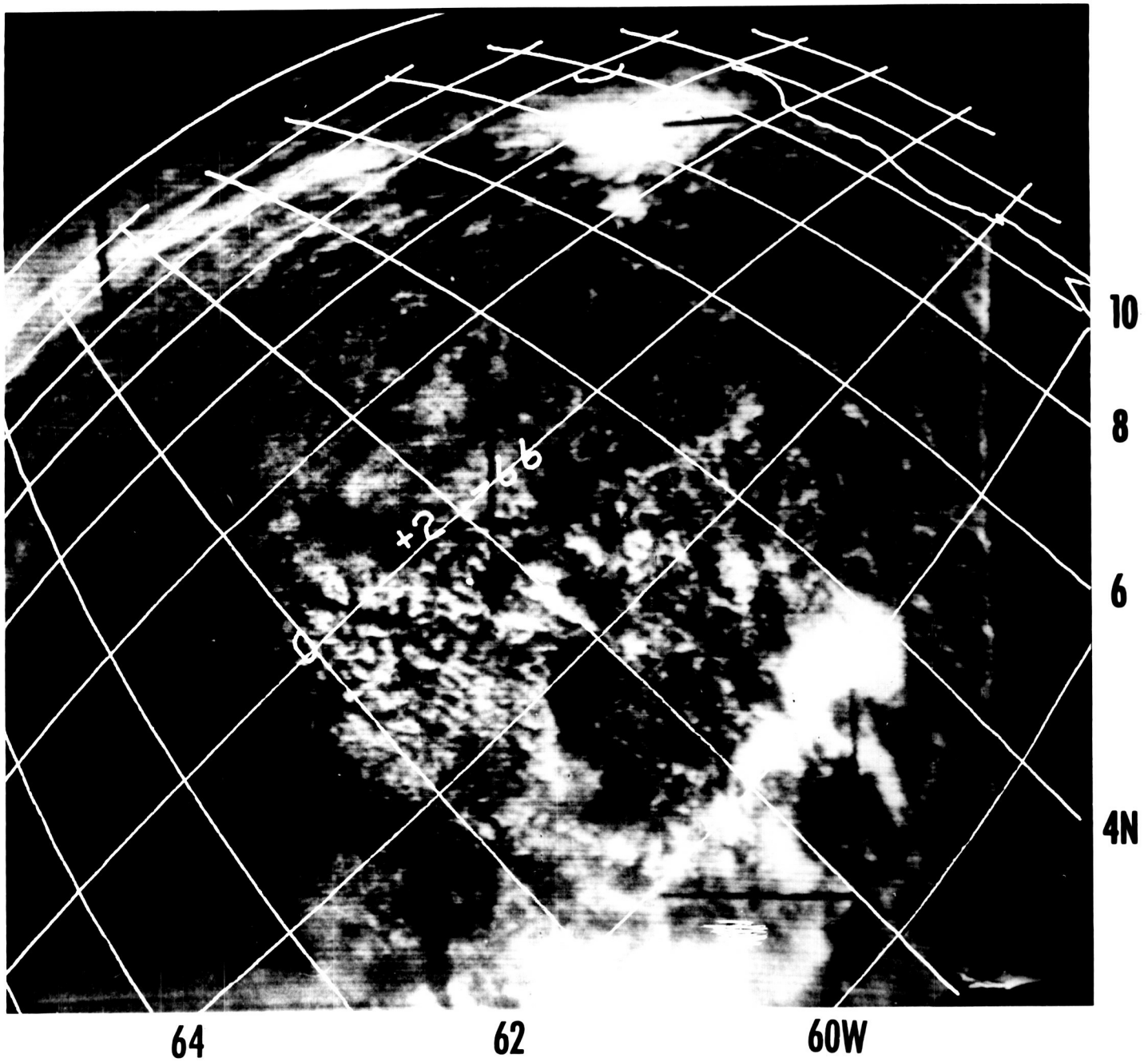
10
8
6
4N
64
62
60W

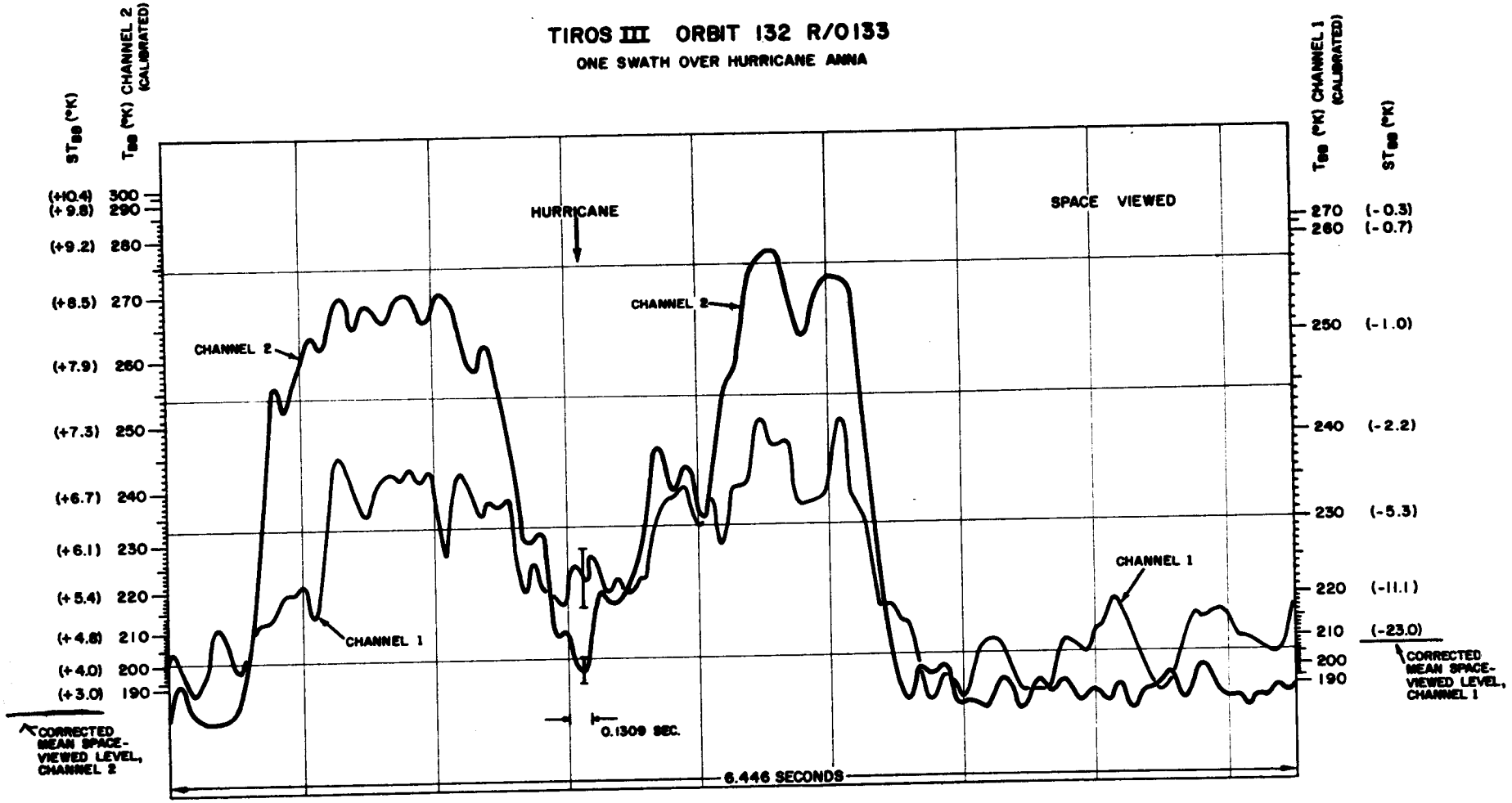
TIROS III ORBIT 132 R/0133
ONE SWATH OVER HURRICANE ANNA
ST_{BB} (°K)
T_{BB} (°K) CHANNEL 2 (CALIBRATED)
(+10.4) 300
(+9.8) 290
(+9.2) 280
(+8.5) 270
(+7.9) 260
(+7.3) 250
(+6.7) 240
(+6.1) 230
(+5.4) 220
(+4.8) 210
(+4.0) 200
(+3.0) 190
CORRECTED MEAN SPACE-VIEWED LEVEL, CHANNEL 2
HURRICANE
SPACE VIEWED
CHANNEL 2
CHANNEL 2
CHANNEL 1
CHANNEL 1
0.1309 SEC.
6.446 SECONDS
T_{BB} (°K) CHANNEL 1 (CALIBRATED)
ST_{BB} (°K)
270 (-0.3)
260 (-0.7)
250 (-1.0)
240 (-2.2)
230 (-5.3)
220 (-11.1)
210 (-23.0)
200
190
CORRECTED MEAN SPACE-VIEWED LEVEL, CHANNEL 1

Fig 16

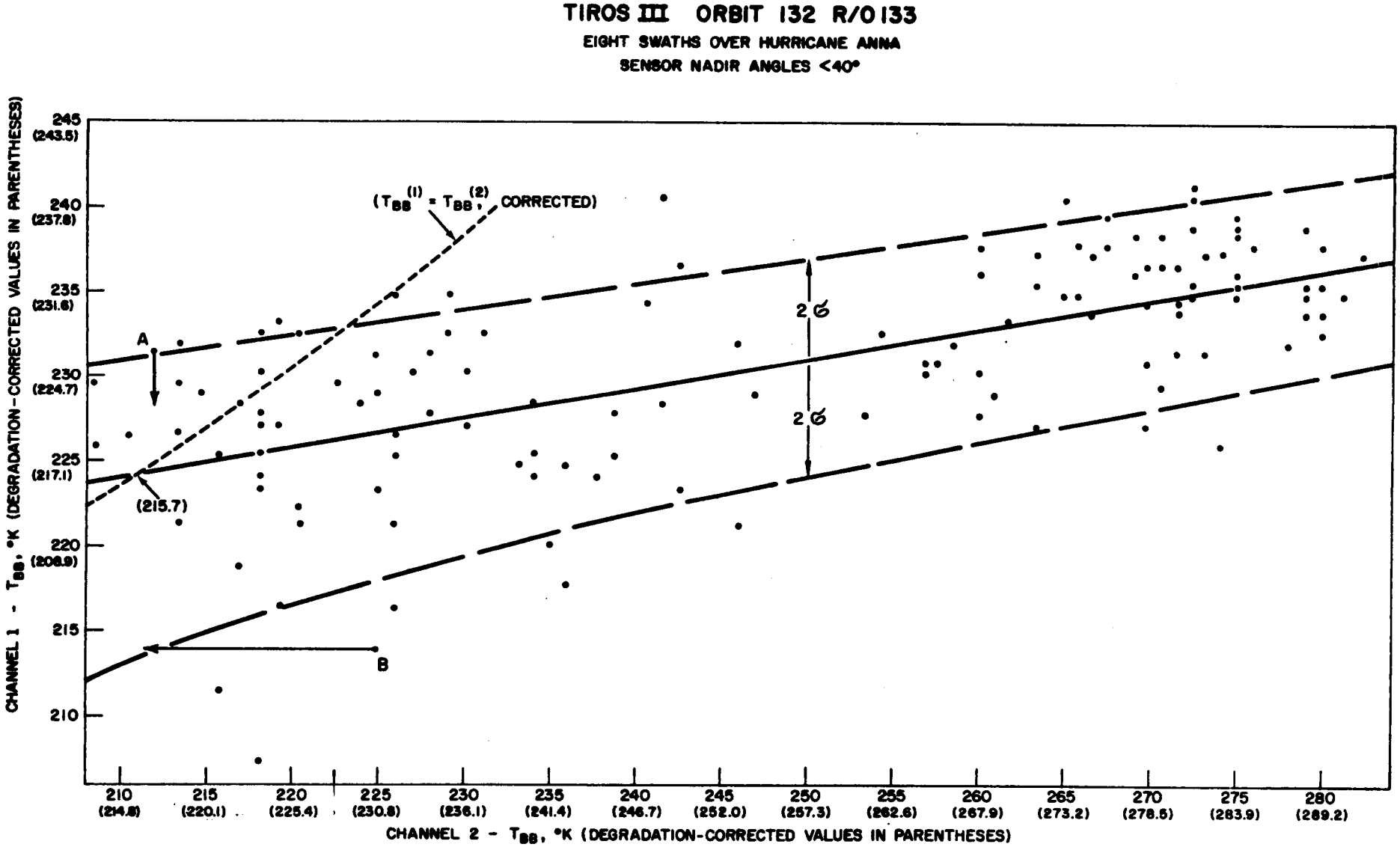
TIROS III ORBIT 132 R/O 133
EIGHT SWATHS OVER HURRICANE ANNA
SENSOR NADIR ANGLES <40°
CHANNEL 1 - T_{BB}, °K (DEGRADATION-CORRECTED VALUES IN PARENTHESES)
245 (243.5)
240 (237.8)
235 (231.6)
230 (224.7)
225 (217.1)
220 (208.9)
215
210
($T_{BB}^{(1)} = T_{BB}^{(2)}$, CORRECTED)
A
B
(215.7)
2σ
2σ
210 (214.8)
215 (220.1)
220 (225.4)
225 (230.8)
230 (236.1)
235 (241.4)
240 (246.7)
245 (252.0)
250 (257.3)
255 (262.6)
260 (267.9)
265 (273.2)
270 (278.5)
275 (283.9)
280 (289.2)
CHANNEL 2 - T_{BB}, °K (DEGRADATION-CORRECTED VALUES IN PARENTHESES)

fig 17

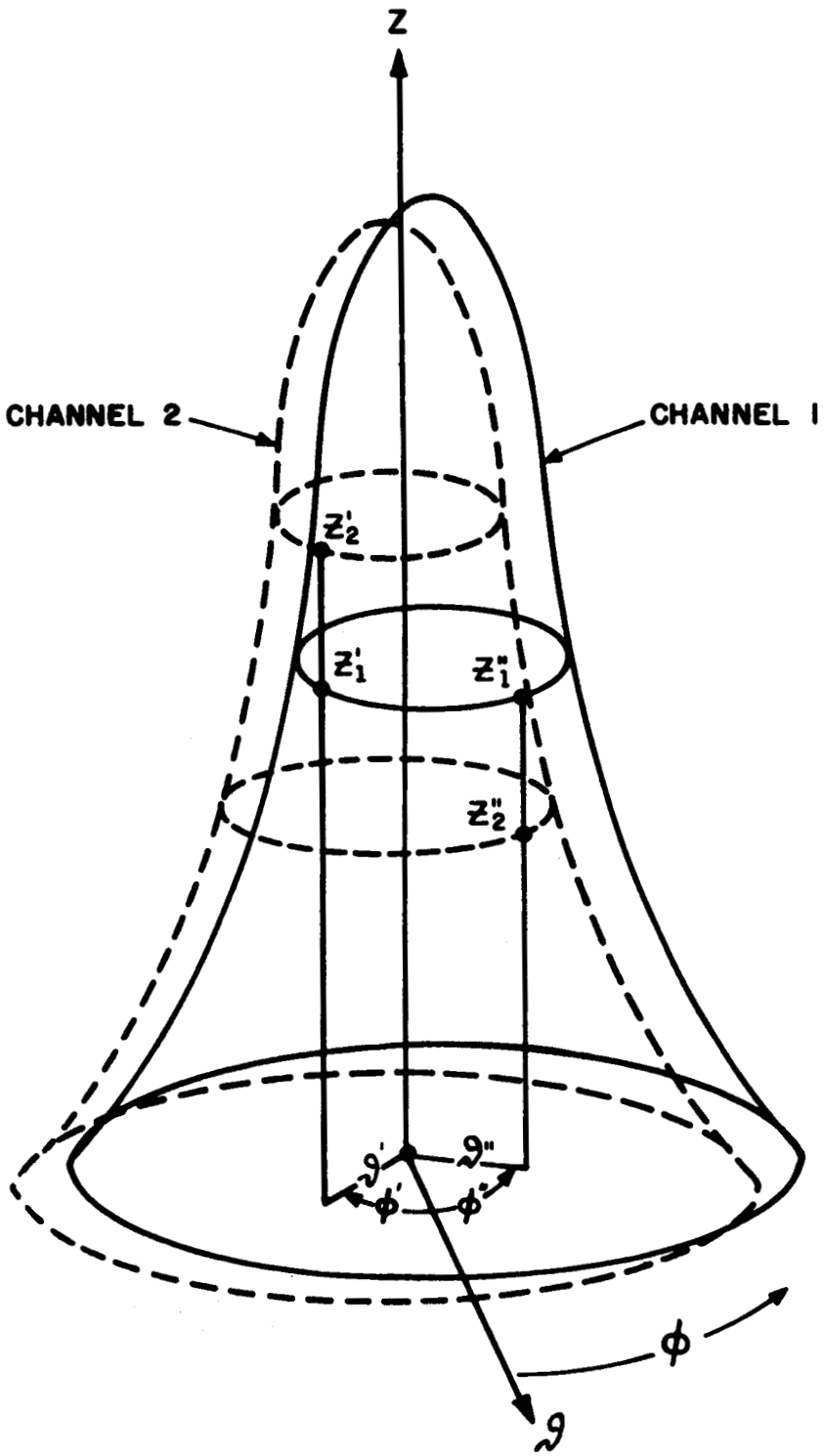
Z
CHANNEL 2
CHANNEL 1
z_2'
z_1'
z_1''
z_2''
ϑ'
ϑ''
ϕ'
ϕ''
ϕ
ϑ

Fig 18